Astrocytes gate long-term potentiation in hippocampal interneurons

Weida Shen[1,6,*], Yejiao Tang[1,2,6], Jing Yang[1,6], Linjing Zhu[1,6], Wen Zhou[1], Liyang Xiang[3,4], Feng Zhu[1], Jingyin Dong[1], Yicheng Xie[5], Ling-Hui Zeng[1,*]

[1] Key Laboratory of Novel Targets and Drug Study for Neural Repair of Zhejiang Province, School of Medicine, Hangzhou City University, Hangzhou, 310015, China
[2] Institute of Pharmacology & Toxicology, College of Pharmaceutical Sciences, Key Laboratory of Medical Neurobiology of the Ministry of Health of China, Zhejiang University, Hangzhou, 310058, China
[3] Zhejiang Key Laboratory of Neuroelectronics and Brain Computer Interface Technology, Hangzhou, 311121, China
[4] School of Medicine, Nankai University, Tianjin, 300071, China
[5] Department of Neurology, The Children's Hospital, Zhejiang University School of Medicine, National Clinical Research Center for Child Health, Hangzhou, 310052, China

[6] These authors contributed equally to this work.
[*] Corresponding authors: Ling-Hui Zeng (zenglh@hzcu.edu.cn), Weida Shen (shenwd@hzcu.edu.cn)

Abstract:

Long-term potentiation is involved in physiological process like learning and memory, motor learning and sensory processing, and pathological conditions such as addiction. In contrast to the extensive studies on the mechanism of long-term potentiation on excitatory glutamatergic synapse onto excitatory neurons ($LTP_{E\rightarrow E}$), the mechanism of LTP on excitatory glutamatergic synapse onto inhibitory neurons ($LTP_{E\rightarrow I}$) remains largely unknown. In the central nervous system, astrocytes play an important role in regulating synaptic activity and participate in the process of $LTP_{E\rightarrow E}$, but their functions in $LTP_{E\rightarrow I}$ remain incompletely defined. Using electrophysiological, pharmacological, confocal calcium imaging, chemogenetics and behavior tests, we studied the role of astrocytes in regulating $LTP_{E\rightarrow I}$ in the hippocampal CA1 region and their impact on cognitive function. We show that $LTP_{E\rightarrow I}$ in stratum oriens of hippocampal CA1 is astrocyte independent. However, in the stratum radiatum, synaptically released endocannabinoids increases astrocyte Ca^{2+} via type-1 cannabinoid receptors, stimulates D-serine release, and potentiate excitatory synaptic transmission on inhibitory neuron through the activation of (N-methyl-D-aspartate) NMDA receptors. We also revealed that chemogentic activation of astrocytes is sufficient to induce NMDA-dependent *de novo* $LTP_{E\rightarrow I}$ in the stratum radiatum of hippocampus. Furthermore, we found that disrupt $LTP_{E\rightarrow I}$ by knockdwon γCaMKII in interneurons of stratum radiatum resulted in dramatic memory impairment. Our findings suggest that astrocytes release D-serine, which activates NMDA receptors to regulate $LTP_{E\rightarrow I}$, and that cognitive function is intricately linked with the proper functioning of this $LTP_{E\rightarrow I}$ pathway.

Keywords: astrocyte; cannabinoid receptor; D-serine; calcium signaling; NMDA receptor; interneuron; synaptic plasticity; γCaMKII; learning and memory

63 **Materials and Methods:**

64 **Animals:**

65 Our study was conducted in accordance with the Guide for the Care and Use of
66 Laboratory Animals and was approved by the ethics committee of the Hangzhou City
67 University (registration number: 22061). C57BL/6 male mice (2-4 months) were
68 purchased from Hangzhou Ziyuan Laboratory Animal Corporation and housed in
69 groups of three to four per cage. The mice were maintained on a 12-hour light/dark
70 cycle and were provided with *ad libitum* access to food and water.

71

72 **Stereotactic virus injection:**

73 Stereotactic virus injection was conducted as described previously (1, 2). Briefly,
74 adult mice were deeply anesthetized with sodium pentobarbital (50 mg/kg) and secured
75 in a stereotaxic device with ear bars (RWD, 68930) while their body temperature was
76 maintained at approximately 37 °C using a heating blanket. Their hair was removed
77 using a razor and the skin was sterilized with iodophor. A 1-cm incision in the midline
78 using sterile scissors. Small burr holes were drilled bilaterally using an electric hand
79 drill at the following coordinates: anteroposterior (AP), 2.3 mm from Bregma;
80 mediolateral (ML), ±1.4 mm. Virus particles were then injected bilaterally into the
81 stratum radiatum (1.2 mm from the pial surface) using glass pipettes connected to an
82 injection pump (RWD, R480). The injection rate was controlled at 1 nl/s using the pump.
83 To allow the virus disseminate into the tissue, glass pipette was left in place for 10
84 minutes after each injection. After the injection, the pipettes were gradually removed
85 and the wound was sutured up. For hippocampal interneuron physiological recording,
86 200 nl AAV2/9 mDLx EGFP (6.4×10^{11} gc/ml) were injected. For hippocampal slice
87 Ca^{2+} imaging, 500 nl AAV2/5 GfaABC$_1$D GCaMP6f (1.2×10^{12} gc/ml) with injected
88 alone or mixed with 500 nl AAV2/5 GfaABC$_1$D hM3D (Gq) mCherry (5.3×10^{12} gc/ml).
89 To knockdown γCaMKII in hippocampal interneuron, an shRNA sequence
90 (5'-GCAGCTTGCATCGCCTATATC-3') was used. A total of 200 nl of AAV2/9 mDLx
91 γCaMKII shRNA (6.4×10^{12} gc/ml) were injected. All virus were generated by Brainvta

92 and Sunbio Medical Biotechnology (Wuhan, https://www.brainvta.tech/ and Shanghai,
93 http://www.sbo-bio.com.cn/).
94
95 **Electrophysiology:**
96 Mice were anesthetized with isoflurane, and their brains were quickly extracted
97 and immersed in an ice-cold solution which containing (in mM) 235 Sucrose, 1.25
98 NaH_2PO_4, 2.5 KCl, 0.5 $CaCl_2$, 7 $MgCl_2$, 20 Glucose, 26 $NaHCO_3$, and 5 Pyruvate (pH
99 7.3, 310 mOsm, saturated with 95% O_2 and 5% CO_2). Coronal hippocampus slices
100 (300-350 μm) were prepared with a vibrating slicer (Leica, V T1200) and incubated for
101 30 - 40 min in artificial cerebrospinal fluid (ACSF) containing (in mM) 26 $NaHCO_3$,
102 2.5 KCl, 126 NaCl, 20 D-glucose, 1 sodium pyruvate, 1.25 NaH_2PO_4, 2 $CaCl_2$ and 1
103 $MgCl_2$ (pH 7.4, 310 mOsm, saturated with 95% O_2 and 5% CO_2).
104
105 The slices were transferred to an immersed chamber and continuously perfused
106 with oxygen-saturated ACSF and GABA receptor blockers, picrotoxin (100 μM) and
107 CGP55845 (5 μM), at a rate of 3 ml/min. Interneurons in the stratum radiatum or
108 stratum oriens were visualized using infrared differential interference contrast and
109 epifluorescence imaging. Perforated-path recordings were conducted as previously
110 described (3). Briefly, perforated whole-cell recording from stratum radiatum or
111 stratum oriens interneurons were made with pipettes filled with solution containing (in
112 mM) 136 K-gluconate, 9 NaCl, 17.5 KCl, 1 $MgCl_2$, 10 HEPES, 0.2 EGTA, 25 μM
113 Alexa 488, amphotericin B (0.5 mg ml^{-1}) and small amounts of glass beads (5–15 μm
114 in diameter; Polysciences, Inc., Warminster, PA, USA) (pH 7.3, 290 mOsm). The
115 pathched neuron was intermittently imaged with epifluorescence to monitor dye
116 penetration. If the patch ruptured spontaneously, the experiment was discontinued.
117
118 Whole-cell voltage-clamp recordings were made from either stratum radiatum or
119 stratum oriens interneurons using pipettes with resistance of 3-4 MΩ and filled with a
120 solution containing (in mM) 4 ATP-Na_2, 0.4 GTP-Na, 125 $CsMeSO_3$, 10 EGTA, 10
121 HEPES, 5 4-AP, 8 TEA-Cl, 1 $MgCl_2$, 1 $CaCl_2$ (pH 7.3–7.4, 280–290 mOsm).

Whole-cell current-clamp recording were made from stratum interneurons using pipettes with resistance of 4 - 6 MΩ and filled with a solution containing (in mM) 125 K-Gluconate, 2 $MgCl_2$, 10 HEPES, 0.4 Na^+-GTP, 4 ATP-Na_2, 10 Phosphocreatine disodium salt, 10 KCl, 0.5 EGTA (pH 7.3–7.4, 280–290 mOsm).

Whole-cell recording were performed on stratum radiatum astrocytes using pipettes with resistance of 8 - 10 MΩ and filled with an intracellular solution containing (in mM) 130 K-Gluconate, 20 HEPES, 3 ATP-Na_2, 10 D-Glucose, 1 $MgCl_2$, 0.2 EGTA (pH 7.3-7.4, 280-290 mOsm). In a subset of experiments, 0.14 mM $CaCl_2$ and 0.45 mM EGTA were included in the upper intracellular solution to maintain a stable level of astrocytic concentration (calculation by Web-MaxChelator) (2, 4).

Electrical stimuli was delivered via theta glass pipettes in the Schaffer Collateral of stratum radiatum, with a 30 s inter-trial interval during baseline and after LTP induction. Evoked EPSPs were recorded in current-clamp model at the resting membrane potential of the stratum radiatum interneuron. After a 10-min stable baseline period, LTP was induced by applying theta-burst stimulation [TBS; five bursts at 200-ms intervals (5 Hz), each burst consisting of five pulses at 100 Hz], paired with five 60-ms long depolarizing steps to -10 mV. Six episodes of TBS paired with depolarization were given at 20-s intervals. In stratum oriens, LTP was induced by applying TBS paired with five 60-ms long hyperpolarizing steps to -90 mV.

sEPSCs were recorded in whole-cell model at -70 mV in the presence of picrotoxin (100 μM) and D-AP5 (50 μM). Paired pulses were delivered at an inter-pulse intervals of 50 ms, and the paired-pulse ratio was calculated by dividing the peak amplitude of the second EPSC by the peak amplitude of first EPSC. To analyze action potential properties, interneurons were recorded at rest and depolarized with 500-ms current injection pulses at 10-pA increments.

152 To avoid NMDAR-mediated signaling rapidly washing out when recording
153 interneuron in whole-cell mode, electrical stimuli was delivered with a 5 s inter-trial
154 interval to measure the I-V relationship for NMDAR-mediated EPSPs within 5 minutes
155 of breaking in. The NMDA/AMPA ratio in the stratum radiatum or stratum oriens
156 interneurons was calculated by measuring the amplitude of NMDAR-mediated EPSCs
157 at + 60 mV (50 ms after stimulation) and the peak amplitude of AMPAR-mediated
158 EPSC recorded at −60 mV. To measure pure NMDAR-mediated EPSCs in interneurons
159 at resting membrane potential in perforated whole-cell recording model, Mg^{2+} free
160 ACSF was used, and D-AP5 (50 μM) and picrotoxin (100 μM) were present in ACSF.
161
162 Axopatch 700B amplifiers were utilized for patch-clamp recordings (Molecular
163 Devices). The data was filtered at 6 kHz and sampled at 20 kHz before being processed
164 off-line using the pClampfit 10.6 program (Molecular Devices). Negative pules (-10
165 mV) were employed to monitor series resistances and membrane resistances. The data
166 was included to analysis if the series resistances varied by less than 20% over the course
167 of the trial. All experiments were carried out at 32°C.
168
169 **Behavioral assays:**
170 For the contextual and cued fear conditioning test, the mouse was habituated to the
171 environment and handled for three consecutive days. On the fourth day, the mice were
172 allowed to explore the conditioning cage for 2 min, after which they received three
173 moderate tone-shock pairs [30 stone (80 dB, 4 kHz) co-terminating with a foot shock
174 (0.4 mA, 2 s)]. Following conditioning, the mice were returned to their home cages.
175 The next day, they were place in the same conditioning cage but without receiving any
176 foot shocks, and their freezing behavior was analyzed for the first 5 min. Four hours
177 after the contextual fear conditioning test, the mice were placed in a novel cage with a
178 different shape and texture of the floors compared to the conditioning cage). They were
179 allowed to freely explore the new environment for 2 min and then subjected to 3 tones
180 stimulations [(80 dB, 4 kHz) lasting for 30 s] separated by intervals of 90s, but without
181 receiving any foot-shocks. Once the final tone had ended, all of the mice were allowed

182 to freely explore the chamber for an additional 90 s. Fear responses were measured by
183 calculating the freezing values of the mice using Packwin software (Panlab, Harvard
184 Apparatus, USA). All apparatus were carefully cleaned with 30% ethanol in between
185 tests.
186
187 **Immunohistochemistry:**
188 Immunohistochemistry was conducted as described previously (1, 5, 6). Briefly,
189 mice were administered a single intraperitoneal injection of 50 mg/kg sodium
190 pentobarbital for anesthesia and were transcardially perfused with phosphate-buffered
191 saline (PBS). After the liver and lungs had become bloodless, the mice were perfused
192 with 4% paraformaldehyde (PFA) in 0.1 M PBS. The brains were quickly removed and
193 placed in 4% PFA at 4°C overnight. Following this, the tissues were cryoprotected in
194 successive concentrations of 10%, 20%, and 30% sucrose before being sliced into 20
195 μm sections using a freezing microtome. After being washed multiple times with PBS,
196 the sections were blocked for 1.5 hours at room temperature (22-24°C) in a blocking
197 solution consisting of 5% Bovine Serum Albumin (BSA) and 1% Triton X-100.
198 Following the blocking step, the sections were incubated with primary antibodies
199 overnight at 4 °C. Antibodies used were as follows: mouse monoclonal anti-GFAP
200 (1/1000， Cell Signaling Technology Cat #3670， RRID:AB_561049), mouse
201 monoclonal anti-NeuN (1/500, Millipore Cat# MAB377, RRID: AB_2298772), mouse
202 monoclonal GAD67 (1/500, Synaptic Systems Cat# 198 006, RRID: AB_2713980).
203 After wash several times in PBS, sections were then incubated with the following
204 secondary antibody: Alexa Fluor 594 goat anti-mouse (1/1000, Cell Signaling
205 Technology Cat# 8890, RRID: AB_2714182) at room temperature for 2 h. Afterwards,
206 the sections were rinsed several times in PBS and incubated with DAPI for 5 minutes
207 at room temperature. Following this, the sections were rinsed again and mounted with
208 Vectashield mounting medium. Images were examined using a confocal laser scanning
209 microscope (Olympus, VT1000) and analyzed using ImageJ (NIH, RRID:
210 SCR_003070).

211

212 **Ca^{2+} imaging:**

213 Ca^{2+} signals in hippocampal astrocytes were observed under a confocal microscopy
214 (Fluoview 1000; Olympus) with a 40x water immersion objective lens (NA = 0.8).
215 GCaMP6f was excited at 470 nm. Astrocytes located in the hippocampal CA1 region
216 and at least 40 μm away from the slice surface were selected for imaging. Images were
217 acquired at 1 frame per 629 ms. Hippocampal slices were maintained in ACSF
218 containing picrotoxin (100 μM), and CGP55845 (5 μM) using a perfusion system. A
219 single theta burst stimulation (TBS) was used to stimulate the neuron. CNO (5 μM) was
220 bath-applied to activate hM3D(Gq)-mediated Ca^{2+} signals. The Ca^{2+} signal analysis
221 was described previously (1, 2, 5, 6). In some experiments, image stacks comprising
222 10-15 optical sections with 1 μM z-spacing were acquired to facilitate the identification
223 of GCaMP6f and hM3Dq (mCherry) co-expression in astrocytes. Briefly, movies were
224 registered using the StackReg plugin of ImageJ to eliminate any x-y drift. Ca^{2+} signals
225 were then analyzed in selected ROIs using the Time Series Analyzer V3 plugin of
226 ImageJ. GCaMP6f fluorescence was calculated as $\Delta F/F = (F-F_0)/F_0$. Mean $\Delta F/F$ of Ca^{2+}
227 signals were analyzed using Clampfit 10.6.

228

229 **Statistics:**

230 All data processing, figure generation, layout, and statistical analysis were
231 performed using Clampfit 10.6, Prism, MATALAB and Coreldraw. To assess the
232 normality of the data, the Shapiro-Wilk test was used. If the results of the test were not
233 statistically significant ($p > 0.05$), the data were assumed to follow a normal distribution,
234 and a paired t-test was employed. On the other hand, if the test was statistically
235 significant, a Wilcoxon Signed Rank Test or Mann-Whitney Ran Sum Test was utilized.
236 To statistically analyze cumulative frequency distributions, the Kolmogorov-Smirnov
237 test was employed. When comparing two groups, either a Wilcoxon signed-rank test or
238 a Student's t-test (paired or unpaired) was used. When comparing three groups, One-
239 way repeated measures (RM) ANOVA followed by Dunnett's post-hoc test was used.

All values were presented as mean ± standard error of the mean (SEM). Data were considered significantly different when the p value was less than 0.05 (*$p < 0.05$, **$p < 0.01$, ***$p < 0.001$). The numbers of cells or mice used in each analysis were indicated in figure legends.

270 **Introduction:**

271 Long-term potentiation (LTP) was originally discovered as a long-term increase in
272 synaptic efficacy at glutamatergic synapses onto granule cells of the hippocampus (7).
273 This form of plasticity has been well documented at CA1 pyramidal cells, where
274 synaptic plasticity can be induced by the activation of postsynaptic (N-methyl-D-
275 aspartate) NMDA receptors (NMDARs), voltage-dependent Ca^{2+} channels , and
276 metabotropic glutamate receptors (mGluRs) (8, 9) . Numerous studies have provided
277 compelling evidence that LTP in hippocampal network occurs not only at excitatory
278 glutamatergic synapse onto excitatory pyramidal and granule cells ($LTP_{E\rightarrow E}$), but also
279 at excitatory glutamatergic synapses onto inhibitory interneurons ($LTP_{E\rightarrow I}$) (10-14).
280 However, the mechanism behind $LTP_{E\rightarrow I}$ remains controversial due to the
281 heterogeneous expression of proteins in various types of hippocampal interneurons and
282 the absence of synaptic spines between excitatory inputs on interneurons (10, 15). Two
283 distinct forms of $LTP_{E\rightarrow I}$, namely NMDARs-dependent LTP and NMDARs-
284 independent $LTP_{E\rightarrow I}$, have been observed in hippocampal interneurons.

285 Astrocytes are the most prevalent glial cell type in the central nervous system
286 (CNS), and play a critical role in regulating the development and function of the
287 nervous system (16, 17). Astrocyte display multipolar branches with numerous micro-
288 processes that allow them to closely associate with blood vessels, neuronal cell bodies
289 and axons, other glial cells and as well as synapses (18-20). They also express varies
290 ion channels, transporters and neurotransmitter receptors (21, 22). With these
291 membrane proteins, they can sense neuronal activity and exhibit increases in
292 intracellular Ca^{2+} in reaction to neurotransmitters and, in turn, they release neuroactive
293 chemicals called gliotransmitters that regulate synaptic transmission and plasticity (17,
294 23-25). Numerous studies have been shown that the release of D-serine, a co-agonist of
295 NMDAR, from astrocytes is capable of enabling LTP in cultures, in slice and as well as
296 in vivo (4, 26-29). Given the growing number of studies demonstrating the direct roles
297 that astrocytes play in regulating $LTP_{E\rightarrow E}$, it is of particular interest to understand
298 whether and how astrocytes in modulation LTP of excitatory postsynaptic currents in
299 interneuron.

In this particular study, our focus was on the interneurons distributed in the stratum radiatum layer of the CA1 region of the hippocampus. Approximately 80% of these interneurons exhibit NMDAR-dependent $LTP_{E\rightarrow I}$ when presynaptic stimulation is paired with postsynaptic depolarization. We found that blocking astrocyte metabolism and clamping of astrocyte Ca^{2+} signaling can prevent the $LTP_{E\rightarrow I}$ in large NMDAR-containing interneurons, which could be rescued by bath application of D-serine. Furthermore, pharmacological and Ca^{2+} imaging studies have shown that astrocytes respond to Schaffer Collateral stimulation with Ca^{2+} increases through activation of type-1 cannabinoid receptors (CB1R), which stimulates the release of D-serine, and further regulates $LTP_{E\rightarrow I}$ through binding to the glycine site of NMDARs. We also found that activating astrocytes with Gq designer receptors exclusively activated by designer drugs (DREADDs) induced a potentiation of excitatory to inhibitory synapses in stratum radiatum. Additionally, knockdown γCaMKII hampered $LTP_{E\rightarrow I}$ in stratum radiatum of hippocampus in brain slice and disrupted contextual fear conditioning memory in vivo. Taken together, these results are the first to indicate that astrocytes are an integral component of a form of long-term synaptic plasticity between glutamatergic neurons and GABAergic interneurons, and that memory is also regulated by $LTP_{E\rightarrow I}$.

330 **Results:**

331 **Astrocyte play a role in the formation of NMDAR-dependent $LTP_{E\rightarrow I}$ in CA1**
332 **stratum radiatum.**

333 To visualize CA1 stratum radiatum interneurons, we delivered an adeno-associated
334 virus serotype 2/9 (AAV2/9) vector encoding EGFP under the control of the
335 interneuronal mDLx promoter (AAV2/9-mDLx-EGFP) to this region (30). Within the
336 virally transduced region, EGFP expression was limited to the interneuron, with high
337 penetrance (>98% of the GAD67 cells expressed EGFP) **(Fig. S1 A-C)** and almost
338 complete specificity (>98% EGFP positive cells were also GAD67 positive) **(Fig. S1**
339 **D)**. These immunostaining results indicate that EGFP expression was limited to the
340 interneuron in the CA1 region of stratum radiatum.

341 We next examined whether expressing EGFP in interneurons affects their
342 membrane properties and synaptic transmission. To examine these, we performed
343 whole-cell patch recordings of $EGFP^+$ interneurons and putative interneurons in the
344 CA1 stratum radiatum of the hippocampus in the presence of GABAA receptor blocker
345 picrotoxin. We found that the excitability and resting membrane potential are no
346 difference between these $EGFP^+$ interneurons and putative interneurons **(Fig. S2 A-C)**.
347 Moreover, we also found that no difference in spontaneous excitatory postsynaptic
348 currents (sEPSC) and paired-pulse ratio (PPR) at 50 ms interpulse intervals between
349 $EGFP^+$ interneurons and putative interneurons **(Fig. S2 D-H)**. These results indicate
350 that AAV injection and expression exogenous protein in interneurons has no effect on
351 the membrane properties and baseline synaptic transmission of interneuron.

352 To avoid some necessary ingredient for $LTP_{E\rightarrow I}$ induction be diluted from the
353 cytoplasm, perforate patch-clamp were used to record EPSPs from CA1 stratum
354 radiatum interneurons. After a 10 min baseline recording, we delivered theta burst
355 stimulation (TBS) consisting of 100 Hz stimulation with 25 pulses, delivered in six
356 trains separated by 20-second intervals. The TBS was applied to induce $LTP_{E\rightarrow I}$ of the
357 excitatory inputs to CA1 interneurons. The interneurons were depolarized to -10 mV
358 using a voltage-clamp model during the TBS delivery. Under this condition, we found
359 that in 8 out of 10 cells were induced $LTP_{E\rightarrow I}$ lasting at least 45 min **(Fig. 1 A-C)**. We

360 repatched 6 of these successful to induction $LTP_{E\rightarrow I}$ cells and randomly patched 2
361 $EGFP^{+}$ in stratum radiatum in the whole-cell voltage-clamp model. The results
362 indicated that all cells showed a linear current-voltage (I-V) curve for AMPAR, as well
363 as a significant component of NMDAR-mediated currents **(Fig. S3)**. In addition, we
364 found that the induction of $LTP_{E\rightarrow I}$ was completely blocked by NMDAR blocker D-
365 AP5 **(Fig. 1 A-C)**. This result confirmed that $LTP_{E\rightarrow I}$ in CA1 stratum radiatum
366 interneurons is NMDAR dependent (31, 32).
367
368 To investigate whether astrocytes were involved in NMDAR-dependent $LTP_{E\rightarrow I}$ in
369 CA1 stratum radiatum interneurons, we treated slice with fluoroacetate (FAC, 5 mM)
370 to block glial metabolism (4, 33). The results showed that the induction of $LTP_{E\rightarrow I}$ was
371 blocked by FAC but not in control slice **(Fig. 1 D-F)**. Next, we tested whether glial
372 metabolism is involved in $LTP_{E\rightarrow I}$ in CA1 stratum orient, which has been shown to
373 depend on calcium-permeable AMPARs (CP-AMPARs) and metabotropic glutamate
374 receptors (mGluRs) (13). We found that the induction of $LTP_{E\rightarrow I}$ is not blocked by FAC
375 in CA1 stratum oriens (**Fig. S4 A-B**). We repatched 6 of these cells (4 cells from control
376 group and 2 cells from FAC treated group) in whole-cell voltage-clamp mode and
377 observed that they exhibited high rectification AMPARs and a small component of
378 NMDAR-mediated current (**Fig. S5**). This observation confirms previous study
379 findings (32, 34). Moreover, we found that the induction of $LTP_{E\rightarrow I}$ is not blocked by
380 D-AP5 in CA1 stratum oriens (**Fig. S4**). Overall, the results indicate that the formation
381 of $LTP_{E\rightarrow I}$ in CA1 stratum radiatum is tightly regulated by astrocyte function. The
382 results in stratum oriens also exclude the possibility that FAC directly affects the
383 metabolism of interneuron which inhibit the formation of $LTP_{E\rightarrow I}$.
384
385 It is commonly accepted that astrocytic calcium signaling plays a pivotal role in
386 triggering the release of gliotransmitters and modulating synaptic transmission (24, 35-
387 38). In addition, it is well documented that astrocytic calcium signaling is necessary to
388 the formation of $LTP_{E\rightarrow E}$ in CA1 stratum radiatum (4, 26). Thus, we tested whether
389 intracellular Ca^{2+} signals are required for the induction of $LTP_{E\rightarrow I}$ in CA1 stratum

390 radiatum. We found that clamping of astrocyte Ca^{2+} concentration significantly
391 suppressed $LTP_{E\rightarrow I}$ **(Fig. 2 A-D)**. Consistent with the previous study in $LTP_{E\rightarrow E}$, supply
392 of D-serine (50 μM) fully rescued NMDAR-dependent $LTP_{E\rightarrow I}$ **(Fig. 2D)**. For the
393 control, when the intracellular Ca^{2+} concentration of astrocytes was not clamped, but
394 the astrocyte was recorded with a glass pipette, $LTP_{E\rightarrow I}$ was indistinguishable from that
395 induced without patching an astrocyte **(Fig. 2D)**. Overall, these results indicate that
396 functional preservation of astrocytic metabolism and Ca^{2+} mobilization is critical for
397 maintaining the induction of $LTP_{E\rightarrow I}$.
398

399 **Astrocytic Ca^{2+} transients, induced by activation of astroglial cannabinoid type 1**
400 **receptors (CB1Rs), are involved in the regulation of $LTP_{E\rightarrow I}$ formation.**

401 Accumulating evidence indicates that neuronal depolarization in the hippocampus
402 induced astrocytic Ca^{2+} transients, which is mediated by the activation of astroglial
403 CB1Rs (39-43). Moreover, it has been shown that astroglial CB1R-mediated Ca^{2+}
404 elevation is necessary for $LTP_{E\rightarrow E}$ in the CA1 region of hippocampus (26). Therefore,
405 we asked whether astroglial CB1Rs-mediated Ca^{2+} elevations are required for
406 hippocampal $LTP_{E\rightarrow I}$. We first analyzed whether TBS could evoke astrocytic Ca^{2+}
407 transient via CB1Rs in the stratum radiatum of hippocampus. In this study, GCaMP6f
408 was used to analyze astrocytic Ca^{2+} signal, which were specifically expressed in
409 astrocytes by using adeno-associated viruses of the 2/5 serotype (AAV 2/5) with the
410 astrocyte-specific $gfaABC_1D$ promoter **(Fig. S6 A)**. Furthermore, the expression was
411 confirmed by immunohistochemistry. Within the virally transduced region, GCaMP6f
412 expression positive cells in CA1 stratum radiatum were also positive to the astrocyte
413 specific marker GFAP **(Fig. S6 A , C-D)**. Co-staining with the neuron marker NeuN
414 showed no overlap with GCaMP6f expression **(Fig. S6 B, E)**. Consistent with
415 previously studies (26, 44), we found that TBS significantly increased the Ca^{2+}
416 signaling in astrocytes of hippocampal slices in the presence of picrotoxin and
417 CGP55845 **(Fig. 3 A-B, F)**. As predicted, the increase in Ca^{2+} signals after TBS were
418 inhibited by the CB1 receptor inhibitor AM251 **(Fig. 3 C-D, F)**. Previous studies have
419 demonstrated that activation of α1- adrenoceptors increases calcium signals (1, 45-49)

420 and triggers the release of D-serine release in the neocortex (50). However, our results
421 show that α1-adrenoceptors receptors are not involved in the Ca^{2+} signal increase
422 observed after TBS **(Fig. 3F)**.

423 Next, we explore whether CB1Rs-mediated Ca^{2+} elevation was accompanied by
424 the formation of $LTP_{E\rightarrow I}$. We found that $LTP_{E\rightarrow I}$ was significantly reduced in AM251
425 treated slice relative to controls **(Fig. 3 G-I)**. Consistent with the above results shown
426 in **Fig. 2D**, $LTP_{E\rightarrow I}$ was rescued by the addition of D-serine in AM251-treated slices
427

428 **D-serine release from astrocyte potentiates NMDAR-mediated synaptic response.**

429 Next, we explored the underlying mechanisms by which astrocytes control the
430 formation of $LTP_{E\rightarrow I}$ in the CA1 stratum radiatum. Our above results indicate that D-
431 serine is a downstream signal pathway of astrocyte Ca^{2+} signal. D-serine, a co-agonist
432 of NMDAR, could be released by astrocytes through Ca^{2+}-dependent exocytosis and
433 regulate the function of NMDAR. It has been shown that the occupancy of synaptic
434 NMDAR co-agonist sites by D-serine is not saturated in CA1 pyramidal cells (26, 51).
435 However, the level of occupancy of synaptic NMDAR co-agonist sites by D-serine in
436 interneurons of CA1 stratum radiatum remains unclear. Furthermore, previous studies
437 have demonstrated that NMDAR-dependent synaptic responses of interneurons in the
438 stratum radiatum display a strong rundown effect under whole-cell mode (31). Thus,
439 we recorded the NMDAR-mediated EPSPs from stratum radiatum interneurons in the
440 perforated-patch configuration in Mg^{2+} free ACSF, which showed no rundown effect in
441 this configuration **(Fig. 4 A-B)**. Bath application of 50 μM D-serine enhanced the
442 NMDAR-mediated EPSPs **(Fig. 4 A-C)**, indicating that the level of D-serine in the
443 excitatory to inhibitory synapse cleft was not saturated to occupy the co-agonist site.
444 Subsequently, we tested whether TBS could increase extracellular level of D-serine and
445 promote NMDAR-mediated synaptic responses. Our results indicated that NDMAR-
446 mediated responses were transiently enhanced after one TBS, and the percentage of
447 potentiation was reduced by pre-treatment hippocampal slice with 50 μM D-serine **(Fig.
448 4 D-F)**. However, disrupting glial metabolism with FAC rendered the percentage of
449 TBS-induced potentiation insensitive to bath application of D-serine **(Fig. 4F)**.

450 Furthermore, the percentage of potentiation in AMPAR-mediated responses after TBS
451 is insensitive to bath application of D-serine, indicating that the enhancement of
452 NMDAR-mediated response by TBS is not due the change of release probability and
453 cell excitability **(Fig. 4F)**. Taken together, our results indicate that D-serine release from
454 astrocyte potentiates NMDAR-mediated responses by binding the co-agonist site and
455 regulates the formation of $LTP_{E\rightarrow I}$.
456

457 **Chemogenetic activation of astrocytes induced E→I synaptic potentiation**

458 The crucial role of astrocytes in $LTP_{E\rightarrow I}$ has been extensively demonstrated in brain
459 slices (Henneberger et al., 2010; Min and Nevian, 2012; Pascual et al., 2005; Perea and
460 Araque, 2007; Suzuki et al., 2011) and in vivo (26). In this study, we aimed to
461 investigate if the activation of astrocytic G protein-coupled receptor (GPCR) pathway
462 could trigger potentiation of E→I synaptic transmission. We utilized an adeno-
463 associated virus serotype 5 (AAV2/5) vector encoding hM3Dq fused to mCherry for
464 the specific activation of astrocytes via clozapine-N-oxide (CNO). To ensure specific
465 expression in astrocytes, the vector was also under the control of the astrocyte-specific
466 gfaABC1D promoter **(Fig. S7)**.

467 To verify whether CNO application could evoke Ca^{2+} transients in astrocytes, we
468 delivered AVV of hM3Dq along with AAV of GCaMP6f, and conducted confocal Ca^{2+}
469 imaging in brain slices. Our results showed that CNO application indeed induced an
470 increase in intracellular Ca^{2+} levels in cells co-expressing hM3Dq and GCaMP6f **(Fig.
471 5 A-D)**. These results suggest that the expression of hM3Dq is selective to astrocytes
472 and can elicit a rise in intracellular Ca^{2+} levels upon administration of CNO.

473 Subsequently, we investigated the impact of astrocytic Gq activation on evoked
474 synaptic events in interneurons of CA1 stratum radiatum induced by Schaffer
475 Collaterals stimulation, both before and after the administration of CNO. Interestingly,
476 we observe that the EPSC amplitude was potentiated by 60% in response to the exact
477 same stimulus in gfaABC1D::hM3Dq slices treated with CNO **(Fig. 5 E-G)**, while no
478 such potentiation was detected in slices obtained from the mice that were injected a
479 control virus (AAV2/5-gfaABC1D::mCherry) **(Fig. 5 E-G)**.

480

481 Previous studies have indicated that the synaptic potentiation triggered by
482 chemogenetic activation of astrocyte is mediated through the release of D-serine by
483 astrocytes, resulting in the activation of NMDARs (52). To verify whether the
484 astrocytic-induced synaptic potentiation between excitatory and inhibitory neurons is
485 mediated by D-serine release from astrocytes and the subsequent activation of
486 NMDARs, we conducted an experiment in which we administered CNO after blocking
487 the NMDARs with D-AP5 or saturating the glycine site of NMDARs with 50 μM D-
488 serine. Our results showed that both the NMDAR blocker D-AP5 and 50 μM D-serine
489 completely inhibited the potentiation in EPSP amplitude observed in response to CNO-
490 induced astrocytic activation **(Fig. 5 H-J)**. Our findings demonstrate, for the first time,
491 that astrocytic activation alone can trigger *de novo* potentiation of synapses between
492 excitatory and inhibitory neurons, and that this potentiation is indeed mediated by the
493 release of D-serine from astrocytes and subsequent activation of NMDARs.

494

495 **$LTP_{E\rightarrow I}$ in CA1 of stratum radiatum is necessary for long-term memory formation**

496 We have previously shown that GABAergic interneurons in hippocampus express
497 high levels of γCaMKII, while αCaMKII, βCaMKII and δCaMKII are expressed at a
498 lower frequency (53). Additionally, studies have demonstrated that γCaMKII expressed
499 in hippocampal parvalbumin positive (PV^+) interneurons and cultured hippocampal
500 inhibitory interneurons is essential for the induction of $LTP_{E\rightarrow I}$ (53, 54). Specifically, in
501 hippocampal PV^+ interneurons, this protein is also vital for the formation of
502 hippocampal-dependent long-term memory in vivo (53). Therefore, we asked whether
503 astrocyte gated $LTP_{E\rightarrow I}$ in CA1 stratum radiatum involved in the hippocampal-
504 dependent long-term memory formation. Several independent groups provide
505 compelling evidence that astroglial CB1R-mediated signaling pathway regulates
506 excitatory synapse formed by excitatory neurons, rather than excitatory synapses
507 between excitatory neurons and interneurons (39-42, 55-57). Thus, to manipulate this
508 pathway may also affect excitatory synapse formed by excitatory neurons. To avoid this
509 side effect, we specifically knockdown of γCaMKII expression in inhibitory neurons of

510 CA1 stratum radiatum by delivering an adeno-associated virus serotype 2/9 (AAV2/9)
511 vector encoding shRNAs against γCaMKII and EGFP under the control of an inhibitory
512 neuron-specific promoter (AAV2/9-mDLx-EGFP-γCaMKII shRNA) through bilateral
513 stereotactic injection. We observed that interneurons identified by the specific markers
514 GAD67 were also positive for EYFP and therefore likely expressed shRNAs, which led
515 to knockdown γCaMKII in these cells **(Fig. S8)**. To confirm that knockdown γCaMKII
516 could hamper the induction of $LTP_{E\rightarrow I}$, the EYFP positive interneurons in CA1 stratum
517 radiatum were recorded in perforated-patch mode. We found that knocking down
518 γCaMKII in CA1 stratum radiatum interneurons impaired $LTP_{E\rightarrow I}$, but $LTP_{E\rightarrow I}$ in the
519 putative interneurons in stratum radiatum of WT mice is unimpaired **(Fig. 6 A-C)**. In
520 addition, robust $LTP_{E\rightarrow I}$ induced by TBS in EYFP positive interneurons injected with
521 AAV-mDLx-scramble shRNA into the CA1 stratum radiatum of hippocampus **(Fig. 6C)**.
522 Moreover, it is worth noting that the resting membrane potential, frequency and
523 amplitude of sEPSC, excitability and PPR recorded from γCaMKII knockdown
524 interneurons did not differ from those recorded from putative interneurons and EYFP
525 positive interneurons (infected with scramble shRNA) **(Fig. S9)**. Taken together, these
526 results indicate that knocking down γCaMKII from interneuron has no effect on their
527 synaptic transmission at baseline, but impaired the induction of $LTP_{E\rightarrow I}$ in these
528 interneurons.

529 Next, we examined the behavioral consequences of destroying astrocyte gated
530 $LTP_{E\rightarrow I}$ in CA1 stratum radiatum. We analyzed contextual fear conditioning memory,
531 which is associated with activation of the hippocampus. We found that no effect of
532 γCaMKII knockdown on exploration of the context before conditioning was observed
533 **(Fig. 6 D-E)**. 24 hours after training, mice were returned to the training box, and
534 freezing was measured at the first 2 min. We found that γCaMKII knockdown mice
535 showed a significantly reduction in freezing during contextual conditioning **(Fig. 6F)**.
536 Consistent with our previous study (53), γCaMKII knockdown in interneurons in CA1
537 stratum radiatum did not produce a significant effect on freezing during tone
538 conditioning at 28 h after training **(Fig. 6G)**. Taken together, our results strongly
539 suggest that astroglial CB1R signaling pathway gated $LTP_{E\rightarrow I}$ in CA1 stratum radiatum

plays a vital role in hippocampus-dependent long-term memory.

570 **Discussion:**

571 In the present study, we identify $LTP_{E\rightarrow I}$ in CA1 stratum radium is tightly control
572 by D-serine release from astrocyte via the astroglial CB1Rs-mediated Ca^{2+} elevation.
573 In addition, knockdown of γCaMKII by specific shRNA in interneurons in CA1 stratum
574 radium causes cognitive function deficit. Taken together, out data support that astrocyte
575 gated $LTP_{E\rightarrow I}$ in CA1 stratum radium plays a critical role in preserve normal cognitive
576 function.

577

578 CB1Rs are widely expressed in various brain regions including hippocampus and
579 detectable in presynaptic terminals (56, 58), postsynaptic terminals (59, 60),
580 intracellular organelles (61, 62) and also on astrocytes (26, 39-42, 55, 57, 63). However,
581 the effects of astroglial CB1R-mediated signaling on synaptic transmission and
582 plasticity is highly debated. It has been shown that exogenous administration of Δ^9-
583 tetrahydro-cannabinol (THC) lead to a temporally prolonged and spatially widespread
584 activation of astroglial CB1 receptors and trigger glutamate release, which activates
585 postsynaptic NMDARs and induces LTD in the CA3–CA1 hippocampal synapses,
586 resulting working memory deficit (57). Araque and colleagues reported that eCB
587 released from depolarized CA1 pyramidal cell activates astroglial CB1Rs with a shorter
588 and localized way and induces glutamate release, which activates lateral presynaptic
589 mGluRs and induces LTP (41, 42). In another study, Robin et al found that high
590 frequency stimulation (HFS) of Schaffer Collateral induces LTP, which is gated by the
591 activation of astroglial CB1Rs and the release of D-serine from astrocytes (26). These
592 diverse consequences by activation of CB1 receptor may be due to different neuronal
593 activity pattern that induce eCB release and different nature of the agonists.
594 Interestingly, it has been discovered that individual hippocampal astrocytes are capable
595 of releasing both ATP/adenosine and glutamate, and that this release occurs in a time-
596 dependent and activity-sensitive manner in response to neuronal interneuron activity
597 (64). These findings suggest that the specific type and intensity of astrocyte stimulation
598 plays a critical role in determining the downstream signaling pathways that are
599 triggered by CB1R activation in astrocytes. Consistent with previous study, we found

600 that the activation of astroglial CB1Rs induces Ca^{2+} elevation and triggers the release
601 of D-serine that binds to postsynaptic NMDAR and induces LTP formation (26). Our
602 results provide evidence that astroglial CB1R-mediated singling not only modulates the
603 E→E synapses, but also regulates E→I synapses.
604
605 The precise mechanisms through which neurons and astrocytes differentially
606 regulate D-serine levels are yet to be fully elucidated (65-67). However, it is evident
607 that astrocytes play a significant role in regulating the availability of D-serine. The
608 enzyme serine racemase catalyzes the conversion of L-serine into D-serine, which was
609 initially found in astrocytes and microglia in the mammalian brain (29, 68, 69). It should
610 be highlighted that serine racemase has also been detected in neurons (70-72). A study
611 showed that, despite a significant reduction in SR protein levels in the brains of
612 neuronal SR knockout mouse brains, the reduction in D-serine levels was minimal,
613 suggesting that neurons are not the exclusive source of D-serine (70) and neurons may
614 produce and release D-serine under certain conditions. Notably, activation of G protein-
615 coupled receptors in astrocytes through chemogenetic means results in increased
616 synaptic transmission, which is dependent on the availability of D-serine (52, 73).
617 Specifically, the release of D-serine, which is regulated by CB1R in astrocytes, is
618 required for Ca^{2+}-dependent modulation of LTP in vivo (26), as well as the threshold
619 and amplitude of dendritic spikes (74). Moreover, recent studies have shown that
620 conditional connexin double knockout (75) or knockdown of α4nAChR (76) in
621 astrocytes can decrease the extracellular concentration of D-serine, which in turn
622 reduces NMDAR-dependent synaptic potentiation. These findings suggest that
623 astrocytes are the primary source of D-serine, which plays a crucial role in modulating
624 the function of NMDARs.
625
626 It is well established that $LTP_{E\rightarrow E}$ observed in the CA1 region of the hippocampus
627 is triggered by activation of NMDARs. However, $LTP_{E\rightarrow I}$ is less studied compared to
628 $LTP_{E\rightarrow E}$, but recent evidence suggests that it also involves the activation of NMDARs
629 (10, 11, 31, 32, 53, 77). There have been reports of NMDAR-dependent $LTP_{E\rightarrow I}$ in

630 various regions of the brain, including the hippocampus and cortex (10, 11). Our results
631 suggest that different synaptic mechanisms are involved in the induction of $LTP_{E\rightarrow I}$ in
632 different subregions of the hippocampus. The stratum radiatum, where interneuorns
633 contain NMDARs, is known to be sensitive to NMDAR-dependent $LTP_{E\rightarrow I}$. In contrast,
634 the stratum oriens, where interneuorns contain CP-AMPARs, appears to rely on the
635 activation of CP-AMPA receptors for $LTP_{E\rightarrow I}$ induction. Notably, our findings suggest
636 that astrocytes contribute to NMDAR signaling in the induction of $LTP_{E\rightarrow I}$ in the
637 stratum radiatum through the modulation of extracellular levels of the co-agonist D-
638 serine. It is worth noting that our study found that prolonged activation of astrocytes
639 via the Gq-DREADD pathway resulted in a substantial and persistent increase in Ca^{2+}
640 events and significantly potentiated EPSP responses. This is in consistent with earlier
641 observations made by other groups regarding $LTP_{E\rightarrow E}$ (52, 73). Above all, the
642 mechanism of $LTP_{E\rightarrow I}$ in stratum radiatum appears to be share by $LTP_{E\rightarrow E}$ observed in
643 the CA1 region.
644
645 A previous study has demonstrated that knocking down γCaMKII from
646 interneurons can disrupt $LTP_{E\rightarrow I}$ and cognitive function (53, 54). Our results confirmed
647 that knocking down γCaMKII in interneurons of the stratum radiatum also leads to
648 disruption of $LTP_{E\rightarrow I}$ and cognitive function. Ma and colleagues showed that
649 hippocampal network oscillations in the gamma and theta bands were significantly
650 weaker in γCaMKII knockout mice compared to wild-type mice, following learning
651 (53). This suggests that impaired experience-dependent oscillations in the hippocampus
652 of γCaMKII PV-KO mice may lead to cognitive dysfunction. In this respect, it will be
653 intriguing to investigate the network oscillation after learning in our condition in the
654 future study.
655
656 In the hippocampus, GABAergic local circuit inhibitory interneurons make up
657 approximately 10-15% of the total neuronal cell population (78). However, these
658 interneurons are diverse in their subtypes, morphology, distribution, and functions (15,
659 79). In our study, we mainly focused on a subpopulation of interneurons in the stratum

radiatum of hippocampus. Although it is unclear which type of interneuron recorded in our study, but our study indicated that most of interneurons in the stratum radiatum do not express CP-AMPARs but express abundant of NMDARs. These findings are in line with a previous study conducted by Lasmsa *et al*. (32). In our study, we observed that approximately 80% of interneurons in stratum radium were able to induce LTP successfully. This finding contrasts with the observation made by Lamsa *et al*., who reported a figure of approximately 52% interneurons capable of inducing LTP. The reason for this discrepancy could be attributed to differences in the induction protocol used in the respective studies.

Our study corroborates earlier research that suggests distinct synaptic mechanisms are involved in LTP induction in the CA1 region of the hippocampus across different subregions (11, 13, 32). However, the major breakthrough of our study is the demonstration that astrocytic function serves as the gating mechanism for $LTP_{E\rightarrow I}$ induction in the stratum radiatum. Additionally, our data reveals that the activation of astrocytes via the Gq-DREADD pathway produces *de novo* long-lasting potentiation of EPSP in stratum radiatum interneurons and the knockdown of γCaMKII disrupts cognitive function. These results shed light on the complex mechanisms underlying learning and memory in the hippocampus, and may have implications for developing new therapies targeted at modulating astrocytic function for the treatment of memory disorders.

690 **References:**

691 1. W. Shen *et al.*, Astroglial adrenoreceptors modulate synaptic transmission and contextual fear
692 memory formation in dentate gyrus. *Neurochem. Int.* **143**, 104942 (2021).
693 2. W. Shen *et al.*, Somatostatin interneurons inhibit excitatory transmission mediated by
694 astrocytic GABAB and presynaptic GABAB and adenosine A1 receptors in the hippocampus. *J.*
695 *Neurochem.* 10.1111/jnc.15662 (2022).
696 3. Y. Z. Liu, Y. Wang, W. Shen, Z. Wang, Enhancement of synchronized activity between
697 hippocampal CA1 neurons during initial storage of associative fear memory. *J. Physiol.* **595**,
698 5327-5340 (2017).
699 4. C. Henneberger, T. Papouin, S. H. Oliet, D. A. Rusakov, Long-term potentiation depends on
700 release of D-serine from astrocytes. *Nature* **463**, 232-236 (2010).
701 5. W. Shen, L. Nikolic, C. Meunier, F. Pfrieger, E. Audinat, An autocrine purinergic signaling controls
702 astrocyte-induced neuronal excitation. *Sci. Rep.* **7**, 11280 (2017).
703 6. L. Nikolic *et al.*, Blocking TNFalpha-driven astrocyte purinergic signaling restores normal
704 synaptic activity during epileptogenesis. *Glia* **66**, 2673-2683 (2018).
705 7. T. V. Bliss, T. Lomo, Long-lasting potentiation of synaptic transmission in the dentate area of the
706 anaesthetized rabbit following stimulation of the perforant path. *J. Physiol.* **232**, 331-356
707 (1973).
708 8. T. V. Bliss, G. L. Collingridge, A synaptic model of memory: long-term potentiation in the
709 hippocampus. *Nature* **361**, 31-39 (1993).
710 9. R. A. Nicoll, A Brief History of Long-Term Potentiation. *Neuron* **93**, 281-290 (2017).
711 10. D. M. Kullmann, K. P. Lamsa, Long-term synaptic plasticity in hippocampal interneurons. *Nat.*
712 *Rev. Neurosci.* **8**, 687-699 (2007).
713 11. D. M. Kullmann, K. P. Lamsa, LTP and LTD in cortical GABAergic interneurons: emerging rules
714 and roles. *Neuropharmacology* **60**, 712-719 (2011).
715 12. A. Asgarihafshejani, E. Honore, F. X. Michon, I. Laplante, J. C. Lacaille, Long-term potentiation
716 at pyramidal cell to somatostatin interneuron synapses controls hippocampal network
717 plasticity and memory. *iScience* **25**, 104259 (2022).
718 13. C. Le Duigou, E. Savary, D. M. Kullmann, R. Miles, Induction of Anti-Hebbian LTP in CA1 Stratum
719 Oriens Interneurons: Interactions between Group I Metabotropic Glutamate Receptors and M1
720 Muscarinic Receptors. *J. Neurosci.* **35**, 13542-13554 (2015).
721 14. J. G. Pelletier, J. C. Lacaille, Long-term synaptic plasticity in hippocampal feedback inhibitory
722 networks. *Prog. Brain Res.* **169**, 241-250 (2008).
723 15. K. A. Pelkey *et al.*, Hippocampal GABAergic Inhibitory Interneurons. *Physiol. Rev.* **97**, 1619-1747
724 (2017).
725 16. C. Escartin, O. Guillemaud, M. A. Carrillo-de Sauvage, Questions and (some) answers on
726 reactive astrocytes. *Glia* **67**, 2221-2247 (2019).
727 17. A. Verkhratsky, M. Nedergaard, Physiology of Astroglia. *Physiol. Rev.* **98**, 239-389 (2018).
728 18. E. A. Bushong, M. E. Martone, Y. Z. Jones, M. H. Ellisman, Protoplasmic astrocytes in CA1
729 stratum radiatum occupy separate anatomical domains. *J. Neurosci.* **22**, 183-192 (2002).
730 19. Y. Xie *et al.*, Astrocyte-neuron crosstalk through Hedgehog signaling mediates cortical synapse
731 development. *Cell Rep.* **38**, 110416 (2022).
732 20. M. Santello, N. Toni, A. Volterra, Astrocyte function from information processing to cognition
733 and cognitive impairment. *Nat. Neurosci.* **22**, 154-166 (2019).

734 21. S. Ciappelloni, C. Murphy-Royal, J. P. Dupuis, S. H. R. Oliet, L. Groc, Dynamics of surface
735 neurotransmitter receptors and transporters in glial cells: Single molecule insights. *Cell Calcium*
736 **67**, 46-52 (2017).
737 22. A. Verkhratsky, C. Steinhäuser, Ion channels in glial cells. *Brain Res. Rev.* **32**, 380-412 (2000).
738 23. A. Araque *et al.* (2014) Gliotransmitters travel in time and space. (Neuron), pp 728-739.
739 24. N. Bazargani, D. Attwell, Astrocyte calcium signaling: the third wave. *Nat. Neurosci.* **19**, 182-
740 189 (2016).
741 25. B. S. Khakh, K. D. McCarthy, Astrocyte calcium signaling: from observations to functions and
742 the challenges therein. *Cold Spring Harb. Perspect. Biol.* **7**, a020404 (2015).
743 26. L. M. Robin *et al.*, Astroglial CB(1) Receptors Determine Synaptic D-Serine Availability to Enable
744 Recognition Memory. *Neuron* **98**, 935-944 e935 (2018).
745 27. Y. Yang *et al.*, Contribution of astrocytes to hippocampal long-term potentiation through
746 release of D-serine. *Proc. Natl. Acad. Sci. U. S. A.* **100**, 15194-15199 (2003).
747 28. J. P. Mothet *et al.*, A critical role for the glial-derived neuromodulator D-serine in the age-
748 related deficits of cellular mechanisms of learning and memory. *Aging Cell* **5**, 267-274 (2006).
749 29. A. Panatier *et al.*, Glia-derived D-serine controls NMDA receptor activity and synaptic memory.
750 *Cell* **125**, 775-784 (2006).
751 30. J. Dimidschstein *et al.*, A viral strategy for targeting and manipulating interneurons across
752 vertebrate species. *Nat. Neurosci.* **19**, 1743-1749 (2016).
753 31. K. Lamsa, J. H. Heeroma, D. M. Kullmann, Hebbian LTP in feed-forward inhibitory interneurons
754 and the temporal fidelity of input discrimination. *Nat. Neurosci.* **8**, 916-924 (2005).
755 32. K. P. Lamsa, J. H. Heeroma, P. Somogyi, D. A. Rusakov, D. M. Kullmann, Anti-Hebbian long-term
756 potentiation in the hippocampal feedback inhibitory circuit. *Science* **315**, 1262-1266 (2007).
757 33. R. A. Swanson, S. H. Graham, Fluorocitrate and fluoroacetate effects on astrocyte metabolism
758 in vitro. *Brain Res.* **664**, 94-100 (1994).
759 34. I. Oren, W. Nissen, D. M. Kullmann, P. Somogyi, K. P. Lamsa, Role of ionotropic glutamate
760 receptors in long-term potentiation in rat hippocampal CA1 oriens-lacunosum moleculare
761 interneurons. *J. Neurosci.* **29**, 939-950 (2009).
762 35. M. De Pitta, N. Brunel, A. Volterra, Astrocytes: Orchestrating synaptic plasticity? *Neuroscience*
763 **323**, 43-61 (2016).
764 36. L. Sancho, M. Contreras, N. J. Allen, Glia as sculptors of synaptic plasticity. *Neurosci. Res.* **167**,
765 17-29 (2021).
766 37. M. Navarrete *et al.*, Astrocytes mediate in vivo cholinergic-induced synaptic plasticity. *PLoS Biol.*
767 **10**, e1001259 (2012).
768 38. J. Goenaga, A. Araque, P. Kofuji, D. Herrera Moro Chao, Calcium signaling in astrocytes and
769 gliotransmitter release. *Front. Synaptic Neurosci.* **15**, 1138577 (2023).
770 39. A. Eraso-Pichot *et al.*, Endocannabinoid signaling in astrocytes. *Glia* **71**, 44-59 (2023).
771 40. J. A. Noriega-Prieto, P. Kofuji, A. Araque, Endocannabinoid signaling in synaptic function. *Glia*
772 **71**, 36-43 (2023).
773 41. M. Navarrete, A. Araque, Endocannabinoids mediate neuron-astrocyte communication.
774 *Neuron* **57**, 883-893 (2008).
775 42. M. Navarrete, A. Araque, Endocannabinoids potentiate synaptic transmission through
776 stimulation of astrocytes. *Neuron* **68**, 113-126 (2010).
777 43. M. Navarrete, A. Diez, A. Araque, Astrocytes in endocannabinoid signalling. *Philos. Trans. R.*

778 *Soc. Lond. B Biol. Sci.* **369**, 20130599 (2014).
779 44. M. W. Sherwood *et al.*, Astrocytic IP(3) Rs: Contribution to Ca(2+) signalling and hippocampal
780 LTP. *Glia* **65**, 502-513 (2017).
781 45. F. Ding *et al.*, alpha1-Adrenergic receptors mediate coordinated Ca2+ signaling of cortical
782 astrocytes in awake, behaving mice. *Cell Calcium* **54**, 387-394 (2013).
783 46. G. R. Gordon *et al.*, Norepinephrine triggers release of glial ATP to increase postsynaptic
784 efficacy. *Nat. Neurosci.* **8**, 1078-1086 (2005).
785 47. L. K. Bekar, W. He, M. Nedergaard, Locus coeruleus alpha-adrenergic-mediated activation of
786 cortical astrocytes in vivo. *Cerebral cortex (New York, N.Y. : 1991)* **18**, 2789-2795 (2008).
787 48. M. Paukert *et al.*, Norepinephrine controls astroglial responsiveness to local circuit activity.
788 *Neuron* **82**, 1263-1270 (2014).
789 49. Y. Oe *et al.*, Distinct temporal integration of noradrenaline signaling by astrocytic second
790 messengers during vigilance. *Nat Commun* **11**, 471 (2020).
791 50. Y. Pankratov, U. Lalo, Role for astroglial alpha1-adrenoreceptors in gliotransmission and control
792 of synaptic plasticity in the neocortex. *Front. Cell. Neurosci.* **9**, 230 (2015).
793 51. T. Papouin *et al.*, Synaptic and extrasynaptic NMDA receptors are gated by different
794 endogenous coagonists. *Cell* **150**, 633-646 (2012).
795 52. A. Adamsky *et al.*, Astrocytic Activation Generates De Novo Neuronal Potentiation and Memory
796 Enhancement. *Cell* **174**, 59-71 e14 (2018).
797 53. X. He *et al.*, Gating of hippocampal rhythms and memory by synaptic plasticity in inhibitory
798 interneurons. *Neuron* **109**, 1013-1028 e1019 (2021).
799 54. X. He *et al.*, A Critical Role for gammaCaMKII in Decoding NMDA Signaling to Regulate AMPA
800 Receptors in Putative Inhibitory Interneurons. *Neurosci. Bull.* **38**, 916-926 (2022).
801 55. I. Fernandez-Moncada, G. Marsicano, Astroglial CB1 receptors, energy metabolism, and
802 gliotransmission: an integrated signaling system? *Essays Biochem.* **67**, 49-61 (2023).
803 56. M. Kano, T. Ohno-Shosaku, Y. Hashimotodani, M. Uchigashima, M. Watanabe,
804 Endocannabinoid-mediated control of synaptic transmission. *Physiol. Rev.* **89**, 309-380 (2009).
805 57. J. Han *et al.*, Acute cannabinoids impair working memory through astroglial CB1 receptor
806 modulation of hippocampal LTD. *Cell* **148**, 1039-1050 (2012).
807 58. P. E. Castillo, T. J. Younts, A. E. Chavez, Y. Hashimotodani, Endocannabinoid signaling and
808 synaptic function. *Neuron* **76**, 70-81 (2012).
809 59. S. Marinelli, S. Pacioni, A. Cannich, G. Marsicano, A. Bacci, Self-modulation of neocortical
810 pyramidal neurons by endocannabinoids. *Nat. Neurosci.* **12**, 1488-1490 (2009).
811 60. A. Bacci, J. R. Huguenard, D. A. Prince, Long-lasting self-inhibition of neocortical interneurons
812 mediated by endocannabinoids. *Nature* **431**, 312-316 (2004).
813 61. D. Jimenez-Blasco *et al.*, Glucose metabolism links astroglial mitochondria to cannabinoid
814 effects. *Nature* **583**, 603-608 (2020).
815 62. A. Gutierrez-Rodriguez *et al.*, Localization of the cannabinoid type-1 receptor in subcellular
816 astrocyte compartments of mutant mouse hippocampus. *Glia* **66**, 1417-1431 (2018).
817 63. C. Ramon-Duaso, A. R. Conde-Moro, A. Busquets-Garcia, Astroglial cannabinoid signaling and
818 behavior. *Glia* **71**, 60-70 (2023).
819 64. A. Covelo, A. Araque, Neuronal activity determines distinct gliotransmitter release from a
820 single astrocyte. *Elife* **7** (2018).
821 65. T. Papouin, C. Henneberger, D. A. Rusakov, S. H. R. Oliet, Astroglial versus Neuronal D-Serine:

822 Fact Checking. *Trends Neurosci.* **40**, 517-520 (2017).
823 66. H. Wolosker, D. T. Balu, J. T. Coyle, Astroglial Versus Neuronal D-Serine: Check Your Controls!
824 *Trends Neurosci.* **40**, 520-522 (2017).
825 67. H. Wolosker, D. T. Balu, J. T. Coyle, The Rise and Fall of the d-Serine-Mediated Gliotransmission
826 Hypothesis. *Trends Neurosci.* **39**, 712-721 (2016).
827 68. E. R. Stevens *et al.*, D-serine and serine racemase are present in the vertebrate retina and
828 contribute to the physiological activation of NMDA receptors. *Proc. Natl. Acad. Sci. U. S. A.* **100**,
829 6789-6794 (2003).
830 69. H. Wolosker, S. Blackshaw, S. H. Snyder, Serine racemase: a glial enzyme synthesizing D-serine
831 to regulate glutamate-N-methyl-D-aspartate neurotransmission. *Proc. Natl. Acad. Sci. U. S. A.*
832 **96**, 13409-13414 (1999).
833 70. M. A. Benneyworth, Y. Li, A. C. Basu, V. Y. Bolshakov, J. T. Coyle, Cell selective conditional null
834 mutations of serine racemase demonstrate a predominate localization in cortical glutamatergic
835 neurons. *Cell. Mol. Neurobiol.* **32**, 613-624 (2012).
836 71. K. Miya *et al.*, Serine racemase is predominantly localized in neurons in mouse brain. *J. Comp.*
837 *Neurol.* **510**, 641-654 (2008).
838 72. Y. Dun *et al.*, Serine racemase expression and D-serine content are developmentally regulated
839 in neuronal ganglion cells of the retina. *J. Neurochem.* **104**, 970-978 (2008).
840 73. Y. Van Den Herrewegen *et al.*, Side-by-side comparison of the effects of Gq- and Gi-DREADD-
841 mediated astrocyte modulation on intracellular calcium dynamics and synaptic plasticity in the
842 hippocampal CA1. *Mol. Brain* **14**, 144 (2021).
843 74. K. Bohmbach *et al.*, An astrocytic signaling loop for frequency-dependent control of dendritic
844 integration and spatial learning. *Nat Commun* **13**, 7932 (2022).
845 75. L. Hosli *et al.*, Decoupling astrocytes in adult mice impairs synaptic plasticity and spatial
846 learning. *Cell Rep.* **38**, 110484 (2022).
847 76. W. Ma *et al.*, Astrocytic α4nAchRs Signaling in the Hippocampus Governs the Formation of
848 Temporal Association Memory. *SSRN Electronic Journal* 10.2139/ssrn.4066805 (2022).
849 77. W. Nissen, A. Szabo, J. Somogyi, P. Somogyi, K. P. Lamsa, Cell type-specific long-term plasticity
850 at glutamatergic synapses onto hippocampal interneurons expressing either parvalbumin or
851 CB1 cannabinoid receptor. *J. Neurosci.* **30**, 1337-1347 (2010).
852 78. M. J. Bezaire, I. Soltesz, Quantitative assessment of CA1 local circuits: knowledge base for
853 interneuron-pyramidal cell connectivity. *Hippocampus* **23**, 751-785 (2013).
854 79. S. A. Booker, I. Vida, Morphological diversity and connectivity of hippocampal interneurons.
855 *Cell Tissue Res.* **373**, 619-641 (2018).
856
857
858
859
860
861
862
863
864
865

Acknowledgments.

This work was supported by grants from key R&D Program Project of Zhejiang (2022C03034), Zhejiang Provincial Natural Science Foundation of China (LQ23C090001), Scientific Research Foundation of Zhejiang University City College, (X-202103), Scientific Research Foundation of Hangzhou City University (J-202325), Science and Technology Department of Zhejiang Province (2021RC051).

Conflict of interest:

The authors declare no competing interests.

Data availability statement:

Data are available from the corresponding author on reasonable request.

Author contributions.

W.S. and L.Z. designed the study; W.S. Y.T. and L.Z. analyzed data, wrote the manuscript; W.S., Y.T. J.Y. and L.Z. carried out most experiments; F.Z. and W.Z. helped with viral injection; Y.X. and J.D. helped with immunohistochemistry; J.D. and F.Z. helped with slice electrophysiology; W.Z. and L.X. helped with data analysis. All authors discussed the results and comments on the manuscript.

Figures:

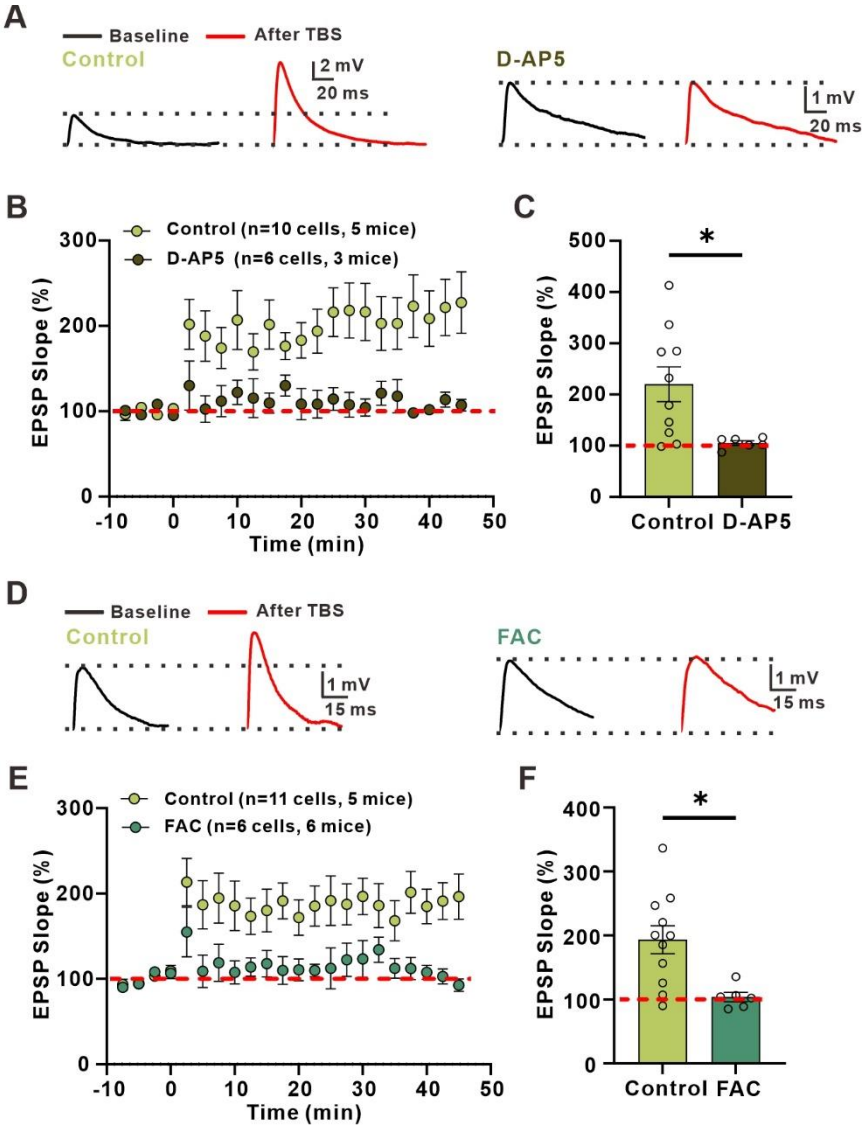

Fig. 1. $LTP_{E\rightarrow I}$ in stratum radiatum is dependent on the activation of NMDA receptor and astrocytic metabolism.

(A) Left: superimposed representative averaged EPSPs recorded 10 min before (dark traces) and 35-45 min after (red traces) LTP induction; Right: superimposed representative averaged EPSPs recorded 10 min before (dark traces) and 35-45 min after (red traces) LTP induction while in the presence of NMDA receptor antagonist D-AP5.

(B) Normalized slope before and after the TBS stimulation protocol in control conditions and in the presence of NMDA receptor antagonist D-AP5.

(C) The summary data measured 35-45 min after LTP induction **(Control: 220.2±33.94,**

n=10 slices from 5 mice; D-AP5: 105.2±4.404, n=6 slices from 3 mice; t=2.580 with 14 degrees of freedom, *p*=0.0218, two-tailed unpaired t-test).

(D) Left: superimposed representative averaged EPSPs recorded 10 min before (dark traces) and 35-45 min after (red traces) LTP induction; Right: superimposed representative averaged EPSPs recorded 10 min before (dark traces) and 35-45 min after (red traces) LTP induction while astrocytic metabolism was disrupted.

(E) Normalized slope before and after the TBS stimulation protocol in control conditions and in the presence of astrocytic metabolism inhibitor FAC.

(F) The summary data measured 35-45 min after LTP induction **(Control: 193.5±21.84, n=11 slices from 5 mice; FAC: 103.8±7.278, n=6 slices from 6 mice; t=2.943 with 15 degrees of freedom, *p*=0.0101, two-tailed unpaired t-test).**

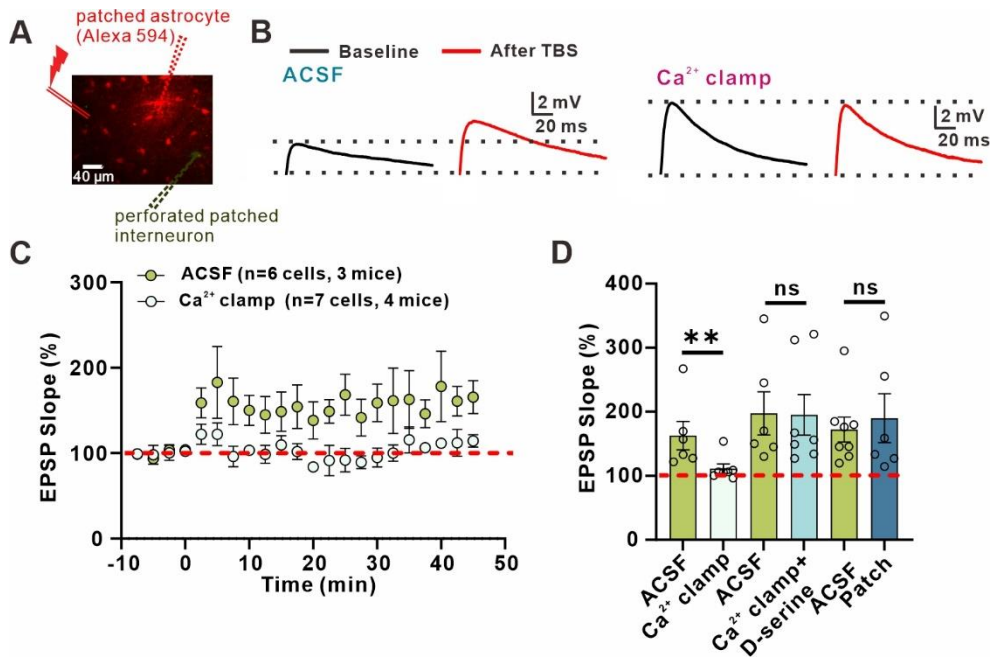

Fig. 2. Astrocyte Ca^{2+} is involved in the induction of $LTP_{E\rightarrow I}$.

(A) Representative image of the astrocytic syncytium illustrating that Ca^{2+} clamping reagents and Alexa Fluor 594 diffuse through gap junctions surround the patched interneuron.

(B) Left: superimposed representative averaged EPSPs recorded 10 min before (dark traces) and 35-45 min after (red traces) LTP induction; Right: superimposed representative averaged EPSPs recorded 10 min before (dark traces) and 35-45 min after (red traces) LTP induction when Ca^{2+} concentration was clamped.

(C) Normalized slope before and after the TBS stimulation protocol in control conditions and when Ca^{2+} concentration was clamped.

(D) The summary data measured 35-45 min after LTP induction **(ACSF: 162.7±22.21, n=6 slices from 3 mice; Ca^{2+} clamp: 111.1±7.323, n=7 slices from 4 mice; Mann-Whitney U Statistic= 3.000, *p*=0.008, Mann-Whitney Rank Sum Test; ACSF: 197.5±33.83, n=6 slices from 4 mice; Ca^{2+} clamp+D-serine: 195.1±31.75, n=7 slices from 4 mice; Mann-Whitney U Statistic= 19.000, *p*=0.836, Mann-Whitney Rank Sum Test; ACSF: 172.2±19.49, n=8 slices from 4 mice; patch: 189.9±38.11, n=6 slices from 3 mice; Mann-Whitney U Statistic= 22.000, *p*=0.852, Mann-Whitney Rank Sum Test).**

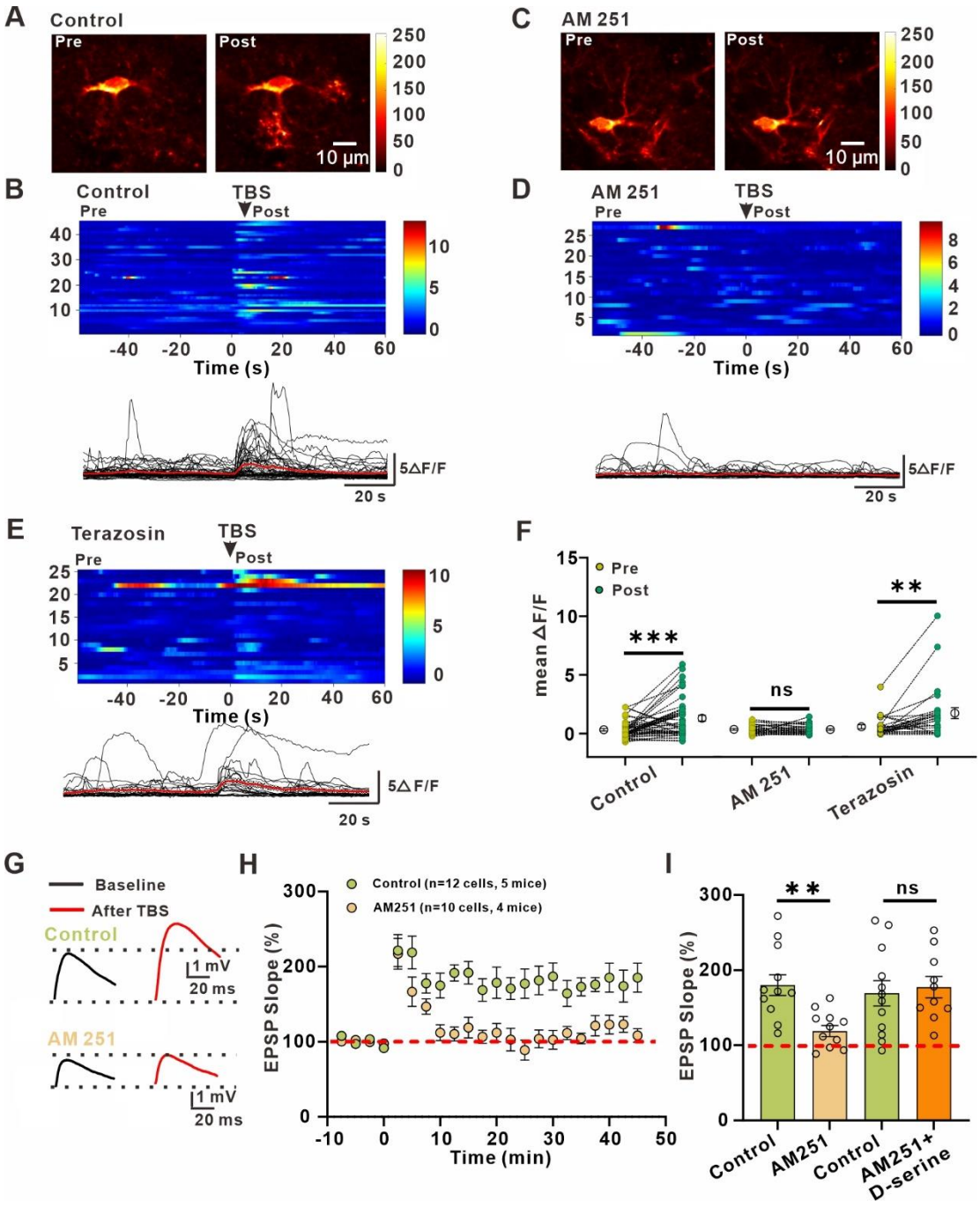

Fig. 3. Activation of astrocytic CB1 receptors causes an increase in astrocytic Ca^{2+} signals and is involved in the induction of $LTP_{E\rightarrow I}$.

(A) Representative images of a GCaMP6f^{+} astrocyte before (left) and after (right) theta burst stimulation (TBS).

(B) Kymographs and △F/F traces of cells with Ca^{2+} signals evoked by the activation of Schaffer collateral with a TBS in GCaMP6f^{+} astrocyte.

(C) Representative images of a GCaMP6f^{+} astrocyte before (left) and after (right) theta

1027 burst stimulation (TBS) when in the presence of CB1 receptor blocker AM251. .
1028 **(D)** Kymographs and △F/F traces of cells with Ca^{2+} signals evoked by the activation
1029 of Schaffer collateral with a TBS in $GCaMP6f^{+}$ astrocyte when in the presence of CB1
1030 receptor blocker AM251.
1031 **(E)** Kymographs and △F/F traces of cells with Ca^{2+} signals evoked by the activation
1032 of Schaffer collateral with a TBS in $GCaMP6f^{+}$ astrocyte when in the presence of α1-
1033 adrenoceptor blocker terazosin.
1034 **(F)** Summary plots for experiments in (B)-(E) illustrating that Ca^{2+} signals elicited by
1035 TBS is mediated by the activation of CB1 receptors **(Control pre: 0.3275±0.1083** △
1036 F/F**, Control post: 1.313±0.2483** △F/F**, n=45 from 20 cells of 5 mice; z= 3.369,**
1037 ***p*<0.001, Wilcoxon Signed Rank Test; AM251 pre: 0.3541±0.07219** △F/F**, AM251**
1038 **post: 0.3418±0.07240** △F/F**, n=28 from 13 cells from 5 mice; z= -0,797, *p*=0.432,**
1039 **Wilcoxon Signed Rank Test; Terazosin pre: 0.5725±0.1749** △F/F**, Terazosin post:**
1040 **1.73±0.4661** △F/F**, n=25 from 11 cells from 4 mice; z=3.215, *p*=0.001, Wilcoxon**
1041 **Signed Rank Test).**
1042 **(G)** Upon: superimposed representative averaged EPSPs recorded 10 min before (dark
1043 traces) and 35-45 min after (red traces) LTP induction; below: superimposed
1044 representative averaged EPSPs recorded 10 min before (dark traces) and 35-45 min
1045 after (red traces) LTP induction while in the presence of CB1 receptor antagonist
1046 AM251.
1047 **(H)** Normalized slope before and after the TBS stimulation protocol in control
1048 conditions and in the presence of CB1 receptor antagonist AM251.
1049 **(I)** The summary data measured 35-45 min after LTP induction **(Control: 180.2±13.76,**
1050 **n=12 slices from 5 mice; AM251: 118.9±7.406, n=10 slices from 4 mice; t=3.697**
1051 **with 20 degrees of freedom, *p*=0.0014, two-tailed unpaired t-test; Control:**
1052 **169.3±16.89, n=12 slices from 6 mice; AM251+D-serine: 177.4±14.27, n=10 slices**
1053 **from 5 mice; t=0.3561 with 20 degrees of freedom, *p*=0.7255, two-tailed unpaired**
1054 **t-test).**
1055
1056
1057

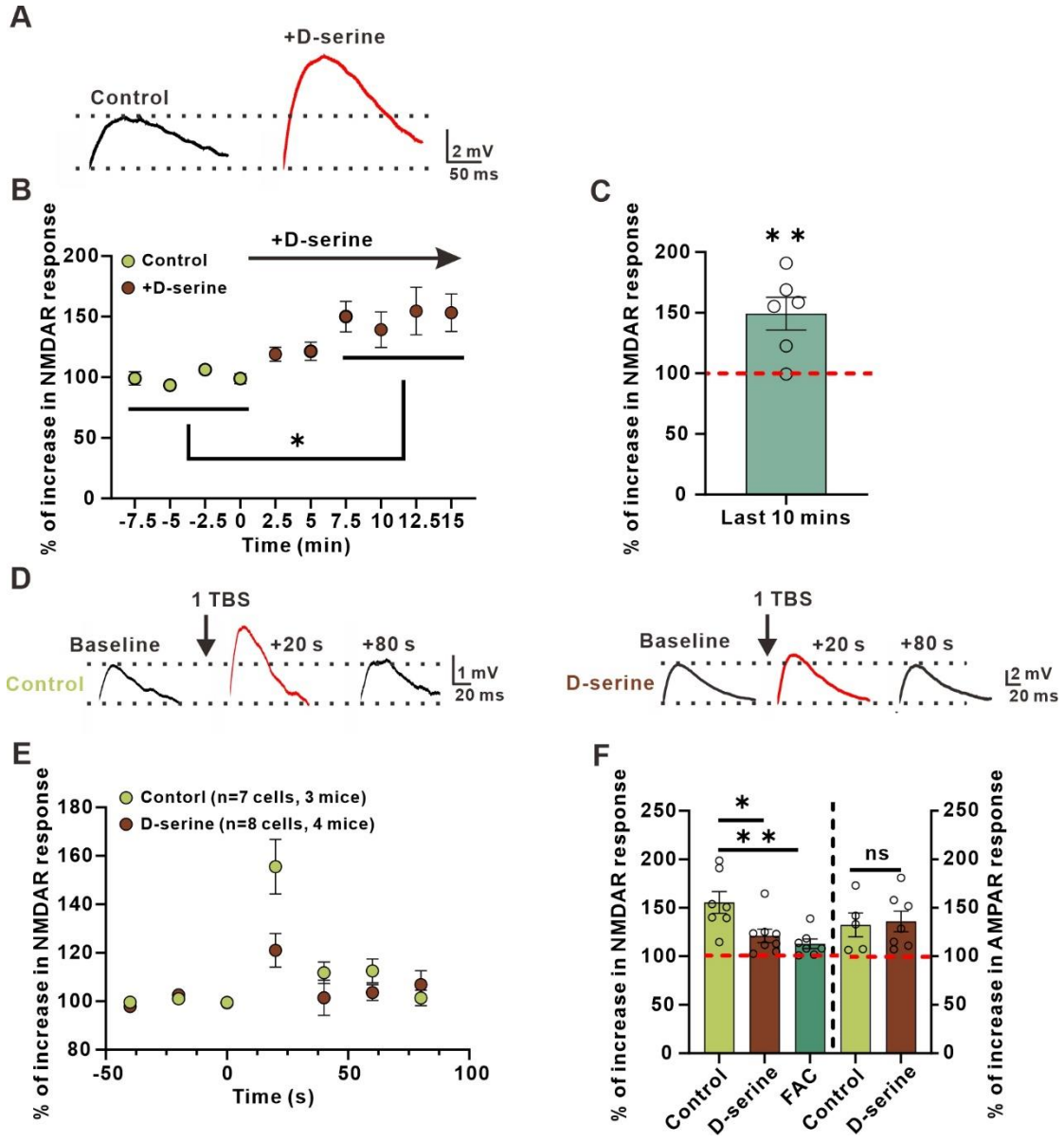

Fig. 4. D-serine release from astrocyte potentiates NMDAR-mediated responses

(A) Example traces of NMDAR-mediated EPSPs before and after bath application of D-serine in stratum radiatum interneurons.

(B) Normalized amplitude before and after add D-serine in stratum radiatum interneurons

(C) The percentage of potentiation in NMDAR-mediated responses **(percentage of potention: 155.523 ± 11.234, n=6 slices from 3 mice; t=-4.942 with 6 degrees of freedom, p=0.00260, two-tailed paired t-test).**

(D) Left: example traces of NMDAR-mediated EPSPs before and after the TBS stimulation protocol in stratum radiatum interneurons .Right: example traces of

NMDAR-mediated EPSPs before and after the TBS stimulation protocol in stratum radiatum interneurons when in the presence of D-serine.

(E) Normalized amplitude before and after the TBS stimulation protocol in stratum radiatum interneurons during ASCF and after application D-serine.

(F) The summary data measured the percentage of potentiation in NMDAR-mediated responses **(Control: 155.5±11.23, n=7 slices from 3 mice; D-serine: 121.1±6.917, n=8 slices from 4 mice; FAC: 112.8±4.931, n=7 slices from 3 mice; *p*=0.0036, F(2, 19)=7.653, ANOVA with Dunnett's comparison) and AMPAR-mediated responses after TBS(Control: 132.357±12.305, n=5 slices from 3 mice; D-serine: 136.012±10.611, n=8 slices from 4 mice; t=-0.224 with 10 degrees of freedom, p=0.827, two-tailed unpaired t-test)**.

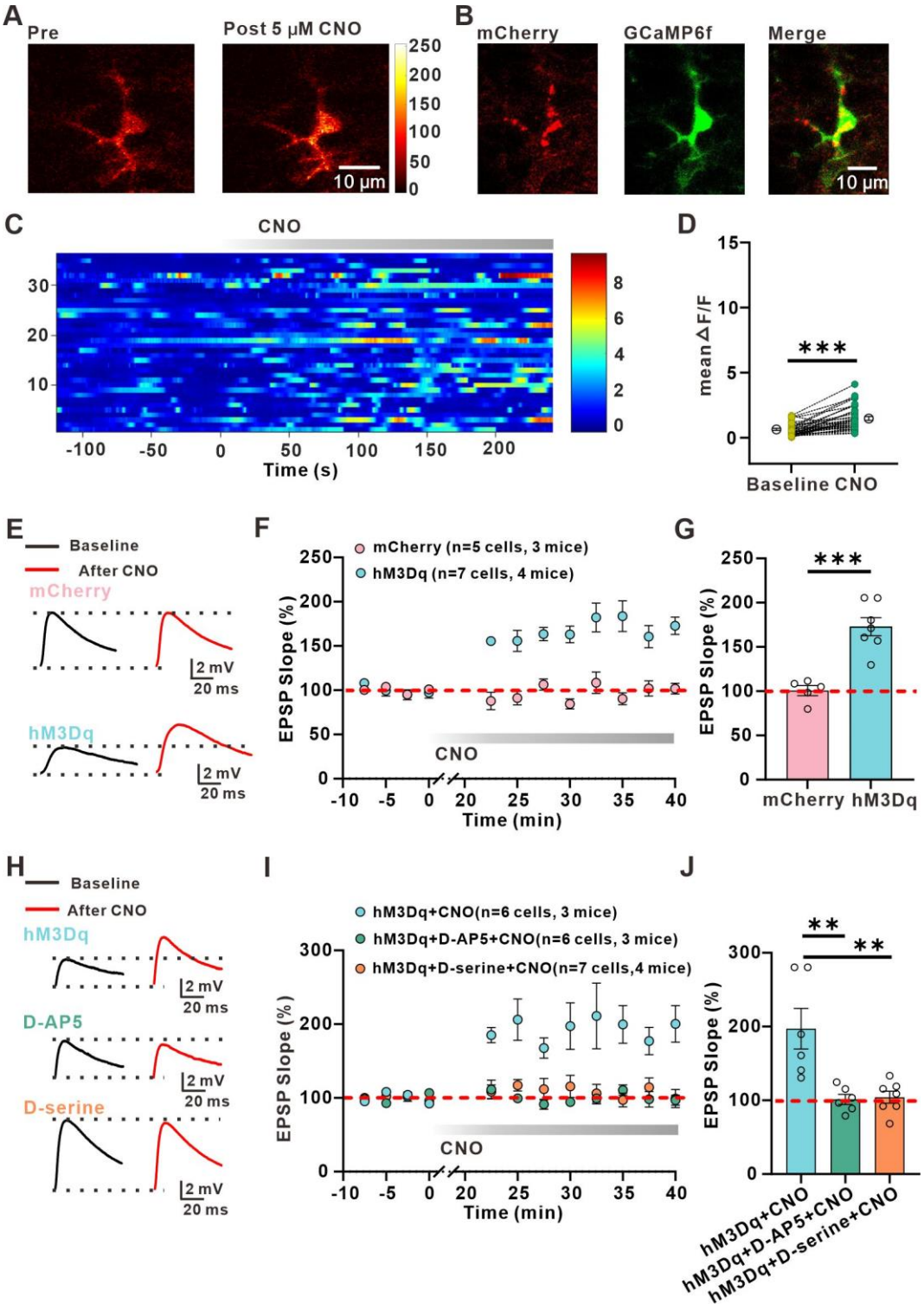

Fig. 5. Astrocytic activation induces *De Novo* LTP$_{E\rightarrow I}$.

(A) Representative images of a GCaMP6f^{+} astrocyte before (left) and after (right) CNO application.

(B) Example confocal images which showing co-expression of GCaMP6f and mCherry constructs confirm that representative cell in (A) is co-expression hM3Dq.

1151 **(C)** Kymographs and △F/F traces of cells with Ca^{2+} signals evoked by bath
1152 application of CNO in $GCaMP6f^{+}$ and $mCherry^{+}$ astrocyte.
1153 **(D)** Summary plot illustrating that CNO is effective to activate astrocytes **(Baseline:**
1154 **0.6167±0.07762** △F/F**, CNO: 1.456±0.1504** △F/F**, n=36 from 19 cells of 3 mice;**
1155 **t=6.411 with 35 degrees of freedom, *p*<0.0001, two-tailed paired t-test)**.
1156 **(E)** Upon: superimposed representative averaged EPSPs recorded 10 min before (dark
1157 traces) and 35-45 min after (red traces) CNO application when astrocyte only express
1158 mCherry; below: superimposed representative averaged EPSPs recorded 10 min before
1159 (dark traces) and 35-45 min after (red traces) CNO applicaion when hM3Dq expressed
1160 astrocytes were activated by CNO
1161 **(F)** Relative EPSP slope before and after CNO application when astrocytes only
1162 express mCherry and when astrocytes express hM3Dq.
1163 **(G)** The summary data measured 35-45 min after LTP induction **(mCherry:**
1164 **100.6±5.651, n=5 slices from 3 mice; hM3Dq: 172.8±10.28, n=7 slices from 4 mice;**
1165 **t=5.474 with 10 degrees of freedom, *p*=0.0003, two-tailed unpaired t-test).**
1166 **(H)** Upon: superimposed representative averaged EPSPs recorded 10 min before (dark
1167 traces) and 35-40 min after (red traces) CNO application; middle: superimposed
1168 representative averaged EPSPs recorded 10 min before (dark traces) and 35-40 min
1169 after (red traces) CNO application when in the presence NMDA receptor blocker D-
1170 AP5; below: superimposed representative averaged EPSPs recorded 10 min before
1171 (dark traces) and 35-40 min after (red traces) CNO application when the glycine sites
1172 of NMDA receptors were saturated by D-serine.
1173 **(I)** Relative EPSP slope before and after CNO application when astrocytes were
1174 activated by CNO, and when in the presence of NMDA receptor antagonist D-AP5 and
1175 in the presence of D-serine.
1176 **(J)** The summary data measured 35-45 min after LTP induction **(hM3Dq+CNO:**
1177 **197.1±27.57, n=6 slices from 3 mice; hM3Dq+CNO+D-AP5: 101.3±6.886, n=6**
1178 **slices from 3 mice; hM3Dq+CNO+D-serine: 104.2+8.166, n=7 slices from 4 mice;**
1179 ***p*=0.0011, F(2, 16)=10.80, ANOVA with Dunnett's comparison).**
1180
1181

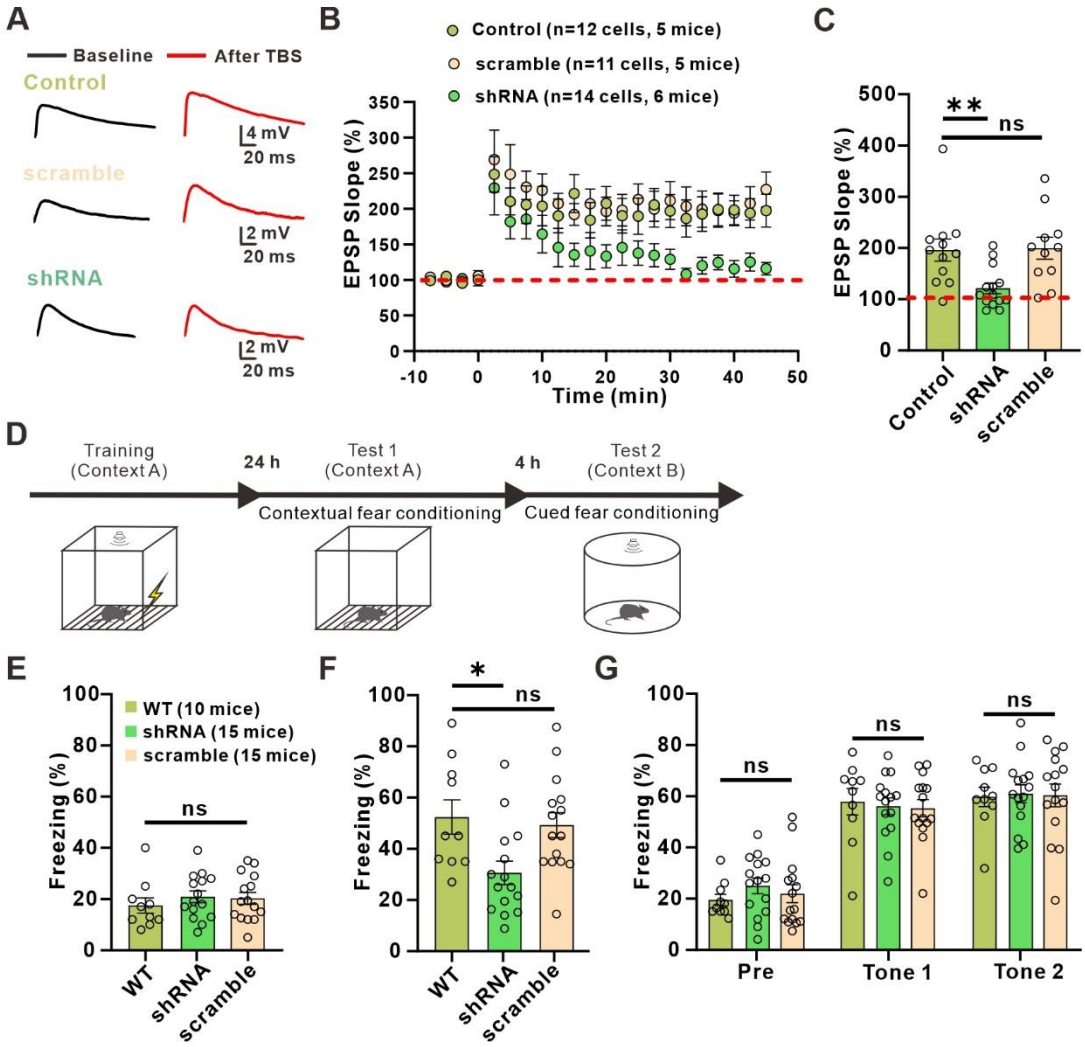

Fig. 6. Impaired hippocampus-dependent long-term memory in knockdown γCaMKII mice

(A) Upon: superimposed representative averaged EPSPs recorded 10 min before (dark traces) and 35-45 min after (red traces) LTP induction in WT group; middle: superimposed representative averaged EPSPs recorded 10 min before (dark traces) and 35-45 min after (red traces) LTP induction in AAV-mDLx-scramble shRNA group; below: superimposed representative averaged EPSPs recorded 10 min before (dark traces) and 35-45 min after (red traces) LTP induction in AAV-mDLx-γCaMKII shRNA group.

(B) Normalized slope before and after the TBS stimulation protocol in control, scramble shRNA and γCaMKII shRNA group.

(C) The summary data measured 35-45 min after LTP induction **(Control: 196±21.56, n=12 slices from 5 mice; γCaMKII shRNA: 121.3±10.64, n=14 slices from 6 mice; scramble shRNA: 199.6±21.42, n=11 slices from 5 mice; *p*=0.0040, F(2, 34)=6.527,**

ANOVA with Dunnett's comparison).

(D) Schematic illustration of the experimental design for contextual and cued fear conditioning test, indicating the time line of the experimental manipulations.

(E) The freezing responses was measured in context A before training in WT, bilaterally injected γCaMKII shRNA and scramble shRNA mice **(Control: 17.5±2.975, n=10 mice; γCaMKII shRNA: 20.9±2.275, n=15 mice; scramble shRNA: 20.29±2.341, n=15 mice; *p*=0.6378, F(2, 37)=0.4553, ANOVA with Dunnett's comparison).**

(F) The freezing responses was measured 24 h after training in WT, bilaterally injected γCaMKII shRNA and scramble shRNA mice **(Control: 52.4±6.695, n=10 mice; γCaMKII shRNA: 30.64±4.574, n=15 mice; scramble shRNA: 49.27±4.899, n=15 mice; *p*=0.0105, F(2, 37)=5.170, ANOVA with Dunnett's comparison).**

(G) The freezing response was measured 28 h after training in WT, bilaterally injected γCaMKII shRNA and scramble shRNA mice **(Pre Control: 19.5±2.171, n=10 mice; Pre γCaMKII shRNA: 25.01±3.016, n=15 mice; Pre scramble shRNA: 21.94±3.519, n=15 mice; *p*=0.4986, F(2, 37)=0.7093, ANOVA with Dunnett's comparison; Tone 1 Control: 57.9±5.153, n=10 mice; Tone 1 γCaMKII shRNA: 56.09±3.319, n=15 mice; Tone 1 scramble shRNA: 55.32±3.368, n=15 mice; *p*=0.9002, F(2, 37)=0.1055, ANOVA with Dunnett's comparison; Tone 2 Control: 59.75±3.825, n=10 mice; Tone 2 γCaMKII shRNA: 60.95±3.482, n=15 mice; Tone 2 scramble shRNA: 60.34±4.485, n=15 mice; *p*=0.9802, F(2, 37)=0.01996, ANOVA with Dunnett's comparison).**

Supporting Figures.

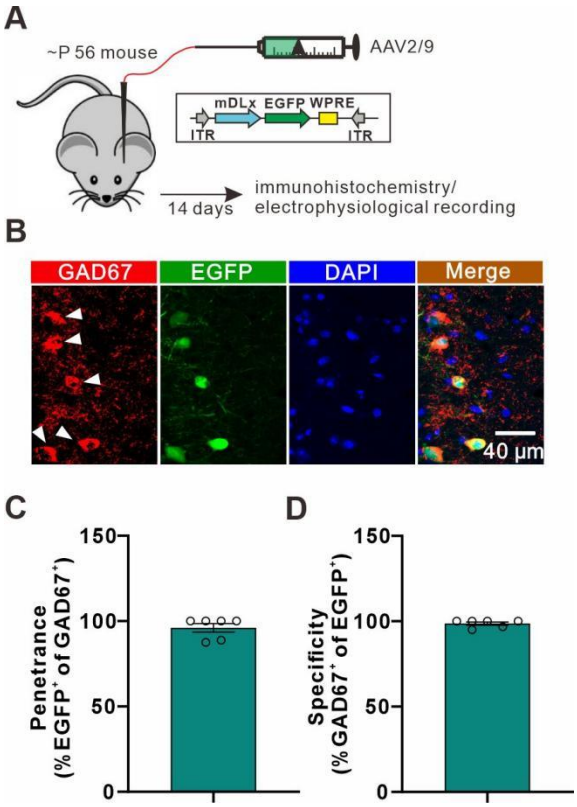

Fig. S1. EGFP is expressed in GABAergic interneurons in the stratum radiatum of hippocampus.

(A) Schematic illustrating the procedure of AAV2/9 microinjections into the stratum radiatum of the hippocampus.

(B) Confocal images showing EGFP (green) and GAD67 (red, white arrow) expressing cells in the stratum radiatum of the hippocampus.

(C and D) mDLx::EGFP was expressed in >98% of interneurons in stratum radiatum of the hippocampus, with >98% specificity.

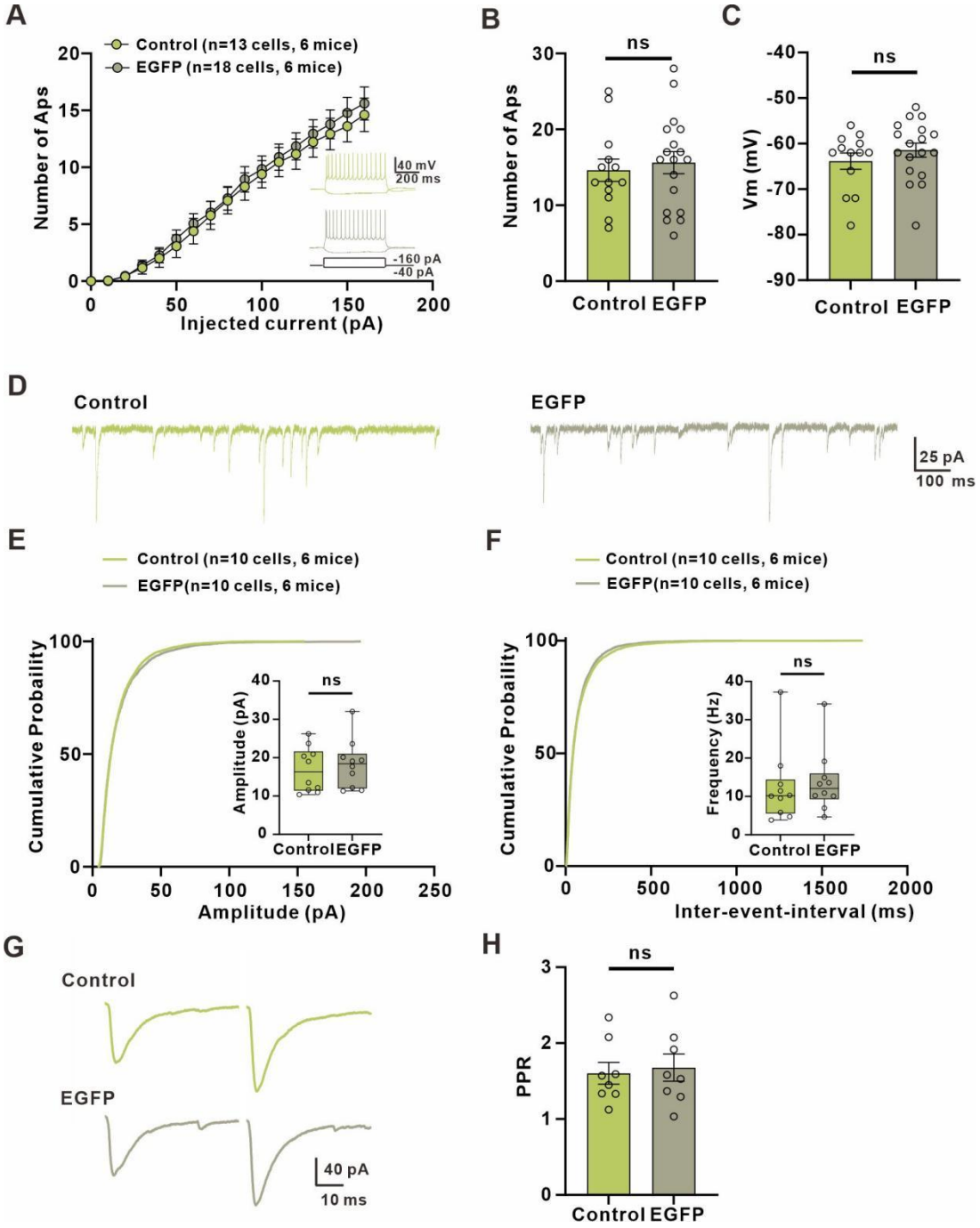

Fig. S2.: EGFP$^+$ interneurons have normal sEPSC, excitability and PPR.

(A) Relationship of injected current to number of APs in postulated interneurons and EGFP$^+$ interneurons. Inset: traces of membrane responses to current injection.

(B) The number of APs at up state membrane potentials (Vm) values **(Control: 14.62±1.474, n=13 slices from 6 mice; EGFP: 15.61±1.458, n=18 slices from 6 mice; ,t=0.4684 with 29 degrees of freedom, *p*=0.643, two-tailed unpaired t-test).**

(C) Interneuron resting membrane potentials **(Control: -63.85±1.779 mV, n=13 slices**

from 6 mice; EGFP: -61.44±1.539 mV, n=18 slices from 6 mice; t=1.018 with 29 degrees of freedom, *p*=0.317, two-tailed unpaired t-test).

(D) Left: example traces of sEPSCs measured in stratum radiatum of hippocampal postulated interneurons of WT mice; Right: example traces of sEPSCs measured in stratum radiatum of hippocampal $EGFP^+$ interneurons of virus injected mice.

(E, F) Cumulative distribution plots and summary of sEPSC amplitude and frequency in postulated interneurons and $EGFP^+$ interneurons **(Amplitude: 16.89±1.846 pA of control, 18.28±2.003 of EGFP, n=10 slices from 6 mice, t=0.5125 with 18 degrees of freedom, *p*=0.6146, two-tailed unpaired t-test; Frequency: 12.41±3.058 Hz of control, 13.78±2.601 Hz of EGFP, n=10 slices from 6 mice, t=0.3405 with 18 degrees of freedom, *p*=0.7374, two-tailed unpaired t-test).**

(G) Example paired-pulse traces measured in postulated interneurons and $EGFP^+$ interneurons.

(H) Summary of paired-pulse ratio **(Control: 1.602±0.1443, n=8 slices from 3 mice; EGFP: 1.677±0.1794, n=8 slices from 3 mice; t=0.3267 with 14 degrees of freedom, *p*=0.7488, two-tailed unpaired t-test).**

.

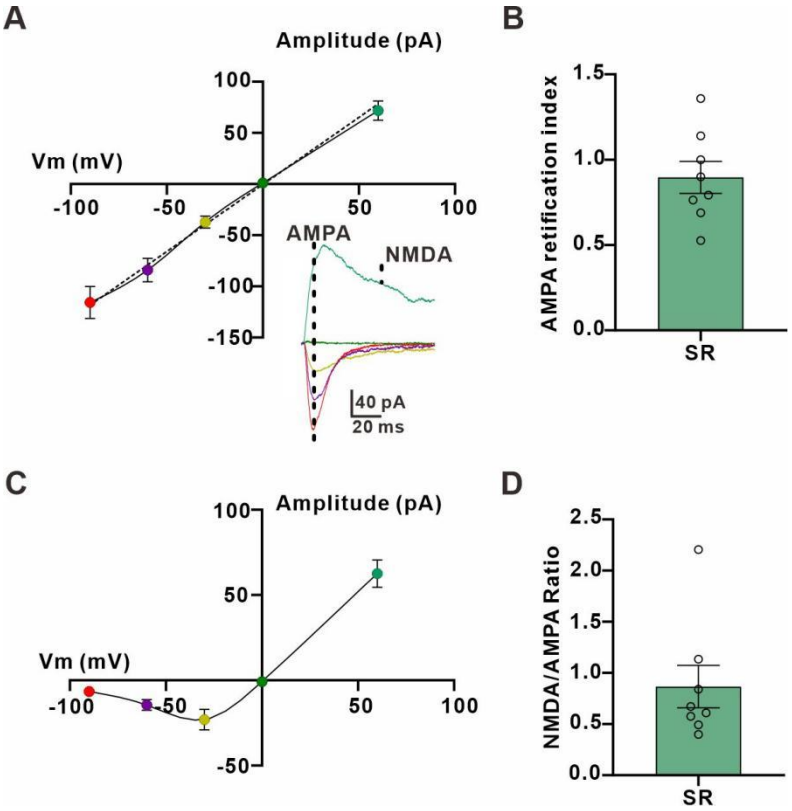

Fig. S3. Stratum radiatum interneurons show linear rectifying AMPARs and a big NMDAR-mediated component.

(A) Current-voltage (I-V) relation of AMPAR-mediated EPSCs in stratum radiatum interneurons. Inset: averaged EPSCs traces at -90, -60, -30, 0 and 60 mV, showing the times at which the two components were measured.

(B) AMPA rectification index (EPSC amplitude at 60 mV / EPSC amplitude at -60 mV) in eight interneurons from stratum radiatum indicates linear rectifying AMPARs **(AMPA retification index: 0.8959±0.09362)**.

(C) I-V relation for the NMDAR-mediated EPSCs in stratum radiatum interneurons.

(D) NMDA / AMPA ratio (NMDAR-mediated EPSC amplitude at 60 mV / AMPAR-mediated EPSC amplitude at -60 mV) in eight cells from stratum radiatum **(NMDA/AMPA ratio: 0.8664±0.2075)**.

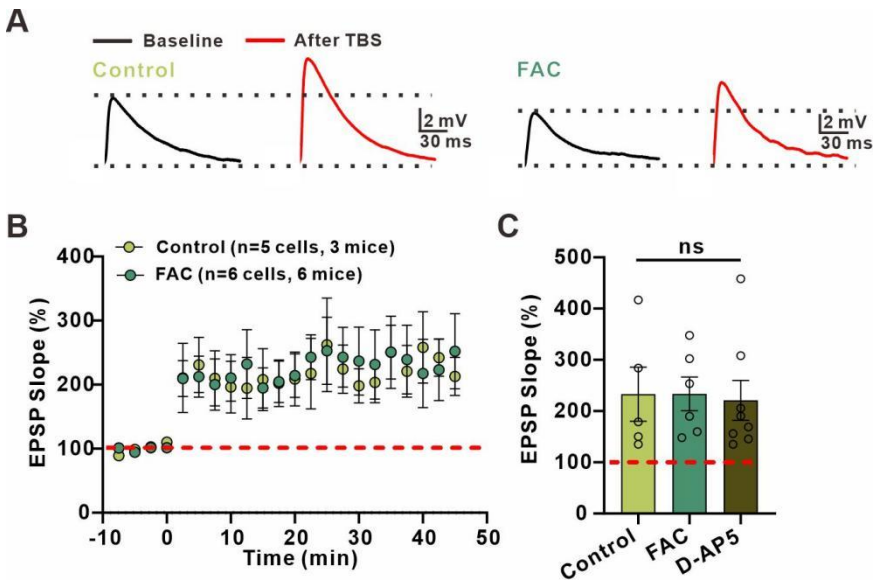

Fig. S4. $LTP_{E\rightarrow I}$ in stratum oriens is not dependent on astrocytic metabolism and the activation of NMDA receptor.

(A) Left: superimposed representative averaged EPSPs recorded 10 min before (dark traces) and 35-45 min after (red traces) LTP induction; Right: superimposed representative averaged EPSPs recorded 10 min before (dark traces) and 35-45 min after (red traces) LTP induction when astrocytic metabolism was disrupted.

(B) Normalized slope before and after the TBS stimulation protocol in control conditions and in the presence of astrocytic metabolism inhibitor FAC.

(C) The summary data measured 35-45 min after LTP induction **(Control: 233±52.74, n=5 slices from 3 mice, FAC: 233.5±33.06, n=6 slices from 6 mice; D-AP5:220.9±38.94, n=8 slices from 4 mice; *p*=0.96, F(2, 16)=0.03277, ANOVA with Dunnett's comparison).**

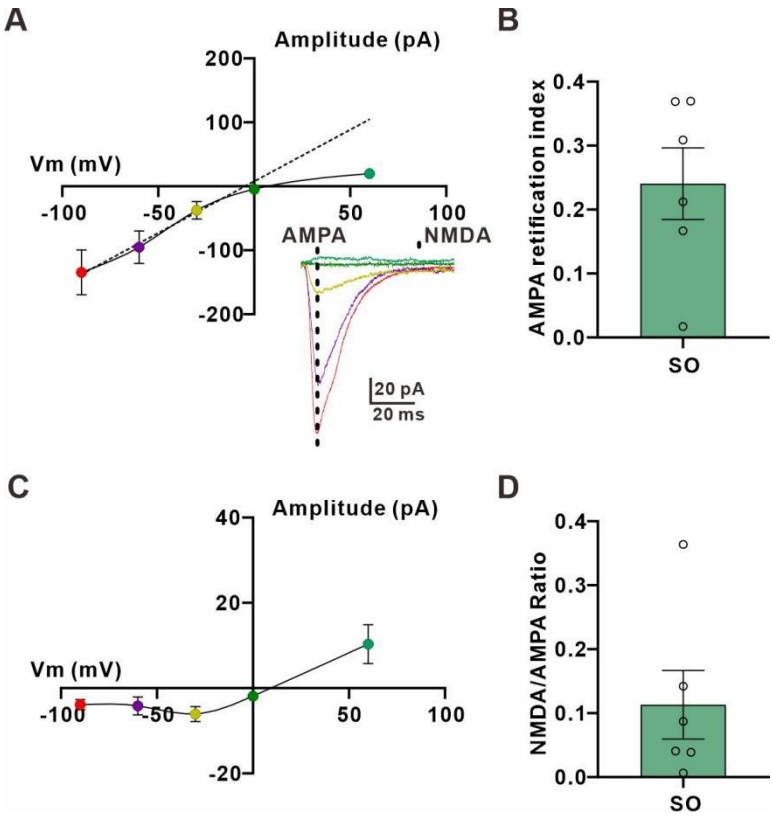

Fig. S5. Stratum oriens interneurons show inwardly rectifying AMPARs and a negligible NMDAR-mediated component.

(A) Current-voltage (I-V) relation of AMPAR-mediated EPSCs in stratum oriens interneurons. Inset: averaged EPSCs traces at -90, -60, -30, 0 and 60 mV, showing the times at which the two components were measured.

(B) AMPA rectification index (EPSC amplitude at 60 mV / EPSC amplitude at -60 mV） in six interneurons from stratum oriens indicate inwardly rectifying AMPARs **(AMPA retification index: 0.2406±0.05594)**.

(C) I-V relation for the NMDAR-mediated EPSCs in stratum oriens interneurons.

(D) NMDA /AMPA ratio (NMDAR-mediated EPSC amplitude at 60 mV / AMPAR-mediated EPSC amplitude at -60 mV) in six cells from stratum oriens **(NMDA/AMPA ratio: 0.1132±0.05370)**.

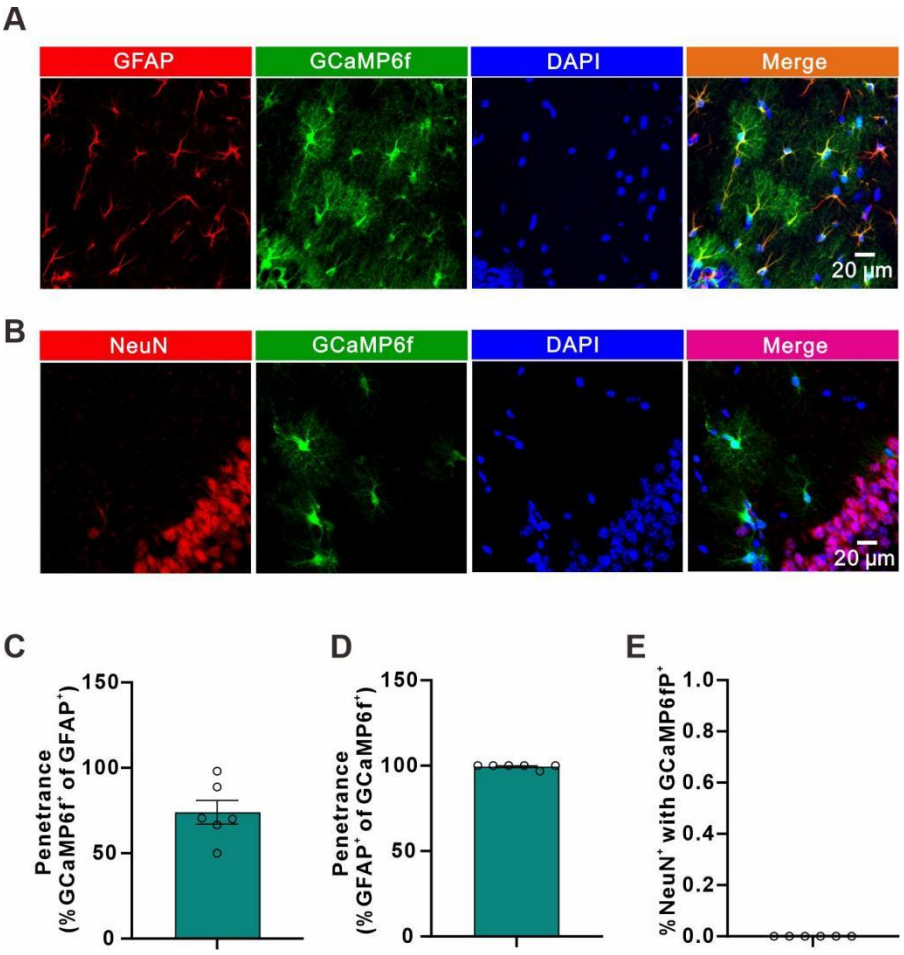

Fig. S6. GCaMP6f was expressed in astrocytes.

(A and B) Representative immunohistochemistry images showing colocalization of GCaMP6f and GFAP (A), but not NeuN (B).

(C and D) gfaABC$_1$D::GCaMP6f was expressed in >70% of astrocyte in stratum radiatum of the hippocampus, with >99% specificity.

(E) Quantification of the percentage of cells expressing NeuN that also expressed GCaMP6f.

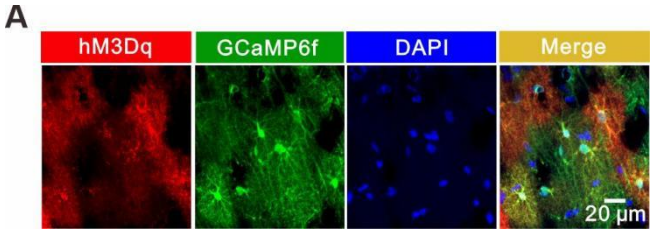

Fig. S7. hM3Dq was expressed in astrocytes.

(A) hM3Dq(mCherry) colocalization with an GCaMP6f in the stratum radiatum of the hippocampus.

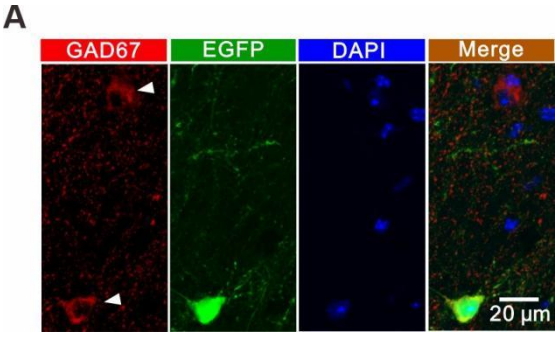

Fig. S8. EGFP-γCaMKII shRNA is expressed in GABAergic interneurons in the stratum radiatum of hippocampus.

(A)Confocal images showing EGFP γCaMKII shRNA (green) and GAD67 (red, white arrows) expressing cells in the stratum radiatum of the hippocampus. These images indicate that the γCaMKII shRNA, which is driven by an interneuron specific promoter (mDLx), is expressed specifically in interneurons.

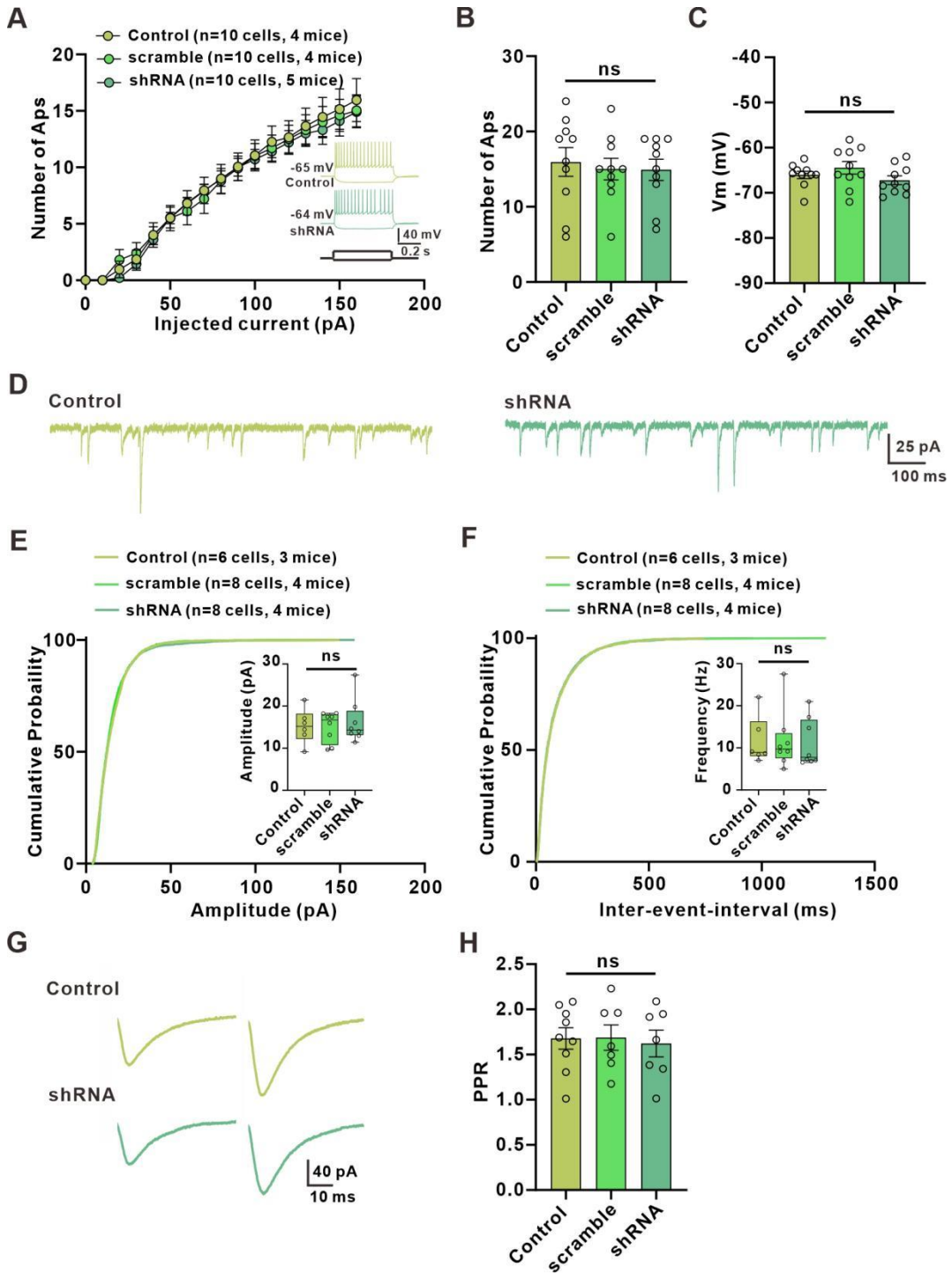

Fig. S9. knockdown γCaMKII from interneurons have no effect on their sEPSC, excitability and PPR

(A) Relationship of injected current to number of APs in postulated interneurons, expressing scramble shRNA and γCaMKII shRNA interneurons. Inset: traces of membrane responses to current injection.

(B) The number of APs at up state membrane potentials (Vm) values **(Control:**

15.95±1.904, n=10 slices from 4 mice; scramble shRNA: 15.00±1.430, n=10 slices from 4 mice; γCaMKII shRNA: 14.90±1.410, n=10 slice from 5 mice; p=0.4986, F(2, 27)=0.4756, ANOVA with Dunnett's comparison).

(C) Interneuron resting membrane potentials **(Control: -66.03±0.8127, n=10 slices from 4 mice; scramble shRNA: -64.44±1.398, n=10 slices from 4 mice; γCaMKII shRNA: -67.23±0.9803, n=10 slice from 5 mice; p=0.2128, F(2, 27)=1.639, ANOVA with Dunnett's comparison)**.

(D) Left: example traces of sEPSCs measured in stratum radiatum of hippocampal postulated interneurons of WT mice; Right: example traces of sEPSCs measured in stratum radiatum of hippocampal $EGFP^+$ interneurons of AAV-mDLx-shRNA γCaMKII expressed mice.

(E, F) Cumulative distribution plots and summary of sEPSC amplitude and frequency in postulated interneurons, expressing scramble shRNA and γCaMKII shRNA interneurons **(Frequency: 11.62±2.328 Hz of control, n=6 slices from 3 mice, 11.69±2.462 Hz of scramble shRNA, n=8 slices from 4 mice, 11.12±2.015 Hz of γCaMKII shRNA, n=8 slices from 4 mice, p=0.9805, F(2, 19)=0.01969, ANOVA with Dunnett's comparison; Amplitude: 15.23±1.846 pA of control, n=6 slices from 3 mice, 14.57±1.382 of scramble shRNA, n=8 slices from 4 mice,16.23±1.821 of γCaMKII shRNA, n=8 slices from 4 mice, p=0.8459, F(2, 19)=0.1688, ANOVA with Dunnett's comparison)**.

(G) Example paired-pulse traces measured in postulated interneurons of WT mice and $EGFP^+$ interneurons of AAV-mDLx-shRNA γCaMKII expressed mice.

(H) Summary of paired-pulse ratio **(Control: 1.679±0.1190 n=9 slices from 3 mice; scramble shRNA: 1.688±0.1405, n=7 slices from 3 mice; γCaMKII shRNA: 1.622±0.1477, n=7 slice from 3 mice; p=0.9361, F(2, 20)=0.06628, ANOVA with Dunnett's comparison)**.